Synthetic seismic model of a Permian biosiliceous carbonate – carbonate depositional system (Spitsbergen, Svalbard Archipelago)

Jafarian, Elham; de Jong, Koos; Kleipool, Lucas M.; Scheibner, Christian; Blomeier, Dierk P.G.; Reijmer, John J.G.

published in
Marine and Petroleum Geology
2018

DOI (link to publisher)
10.1016/j.marpetgeo.2018.01.034

document version
Publisher's PDF, also known as Version of record

Marine and Petroleum Geology 92 (2018) 78–93

Contents lists available at ScienceDirect

Marine and Petroleum Geology

journal homepage: www.elsevier.com/locate/marpetgeo

Research paper

Synthetic seismic model of a Permian biosiliceous carbonate – carbonate depositional system (Spitsbergen, Svalbard Archipelago)

Elham Jafarian[a,*], Koos de Jong[a], Lucas M. Kleipool[a], Christian Scheibner[b], Dierk P.G. Blomeier[c,d], John J.G. Reijmer[a,e]

[a] VU University Amsterdam, Faculty of Earth and Life Sciences, Sedimentology and Marine Geology Group, De Boelelaan 1085, 1081 HV Amsterdam, The Netherlands
[b] Universität Bremen, Geowissenschaften, FB 5, Postfach 330440, D 28334 Bremen, Germany
[c] Norwegian Polar Institute, Geo Department, FRAM Centre, N-9296 Tromsø, Norway
[d] Millennia Stratigraphic Consultants, Germany
[e] College of Petroleum Engineering & Geosciences, King Fahd University of Petroleum & Minerals, Dhahran 31261, Saudi Arabia

ARTICLE INFO

Keywords:
Synthetic seismic
Acoustic properties
Spiculitic chert
Carbonate factories
Spitsbergen

ABSTRACT

The non-unique correspondence between seismic and subsurface geology is a fundamental problem when interpreting seismic data sets. Synthetic seismic models of outcrop analogs are commonly constructed to cover the gap between the small-scale outcrop observations and low-resolution seismic data.

The Permian biosiliceous carbonate – carbonate sediments on Spitsbergen are characterized by a wide variability in lithologies and microfacies determining the petrophysical properties (e.g., porosity, acoustic properties) that consequently complicate seismic interpretation. This study uses 1D and 2D synthetic seismic modelling techniques (at different resolutions) to gain an understanding of how seismic reflectors are expressed with respect to the sediment distribution, aiming to facilitate real seismic interpretation.

In the study area, nine microfacies were defined that were used to produce a geological model displaying small-scale microfacies variations within a well-defined sequence stratigraphic framework. Laboratory derived petrophysical properties (Vp, ρBulk and AI) were assigned to each predefined microfacies body in the geological models in order to construct acoustic impedance models that were used to produce synthetic seismograms.

The appearance of the seismic reflectors in the synthetic seismic profiles is primarily controlled by changes in mineral composition and link to spatial microfacies distributions within the depositional sequences. Differences in acoustic impedance and the origin of synthetic seismic reflections within a single microfacies type are mainly caused by porosity contrasts (varying between 5 and 20%) and diagenetic modifications such as chertification and cementation. This detailed information cannot be derived from the low-frequency seismograms (25–100 Hz) resulting in changes in seismic expression when seismic resolution diminishes.

Comparison with time equivalent, real and synthetic seismic data of the Finnmark Platform reveals similarities with the synthetic seismic reflection patterns of Spitsbergen. In both areas, the pronounced seismic traces follow abrupt microfacies transitions, which are coherent with cycle boundaries and timelines.

1. Introduction

Field-based studies are fundamental for understanding sedimentary systems e.g., geometry, the lateral and vertical heterogeneity of the sediments. Continuous exposures allow for observations at all scales (mm to km) and provide insights into the small-scale heterogeneities within a sequence stratigraphic framework (Janson et al., 2007; Schwab et al., 2007; Zeller et al., 2014). An outcrop-based analysis is the most convenient method to identify the best exploration and production techniques in the hydrocarbon industry. Synthetic seismic models derived from outcrop studies can be of use for comparison with seismic datasets (Zeller et al., 2014, 2015).

Accurate interpretation of low-resolution seismic data is one of the main factors of successful hydrocarbon exploration programs (Bacon et al., 2007). However, indirect measurements of seismic data and mostly incorrect prediction of subsurface geology are the fundamental potential problems in seismic interpretation (Alves et al., 2014; May and Hron, 1978). A method to calibrate and ground-truth seismic analysis is to construct synthetic seismic models resulting from a predefined geological framework and associated petrophysical data

* Corresponding author.
E-mail address: e.jafarian@vu.nl (E. Jafarian).

https://doi.org/10.1016/j.marpetgeo.2018.01.034
Received 13 April 2017; Received in revised form 31 October 2017; Accepted 25 January 2018
Available online 31 January 2018
0264-8172/

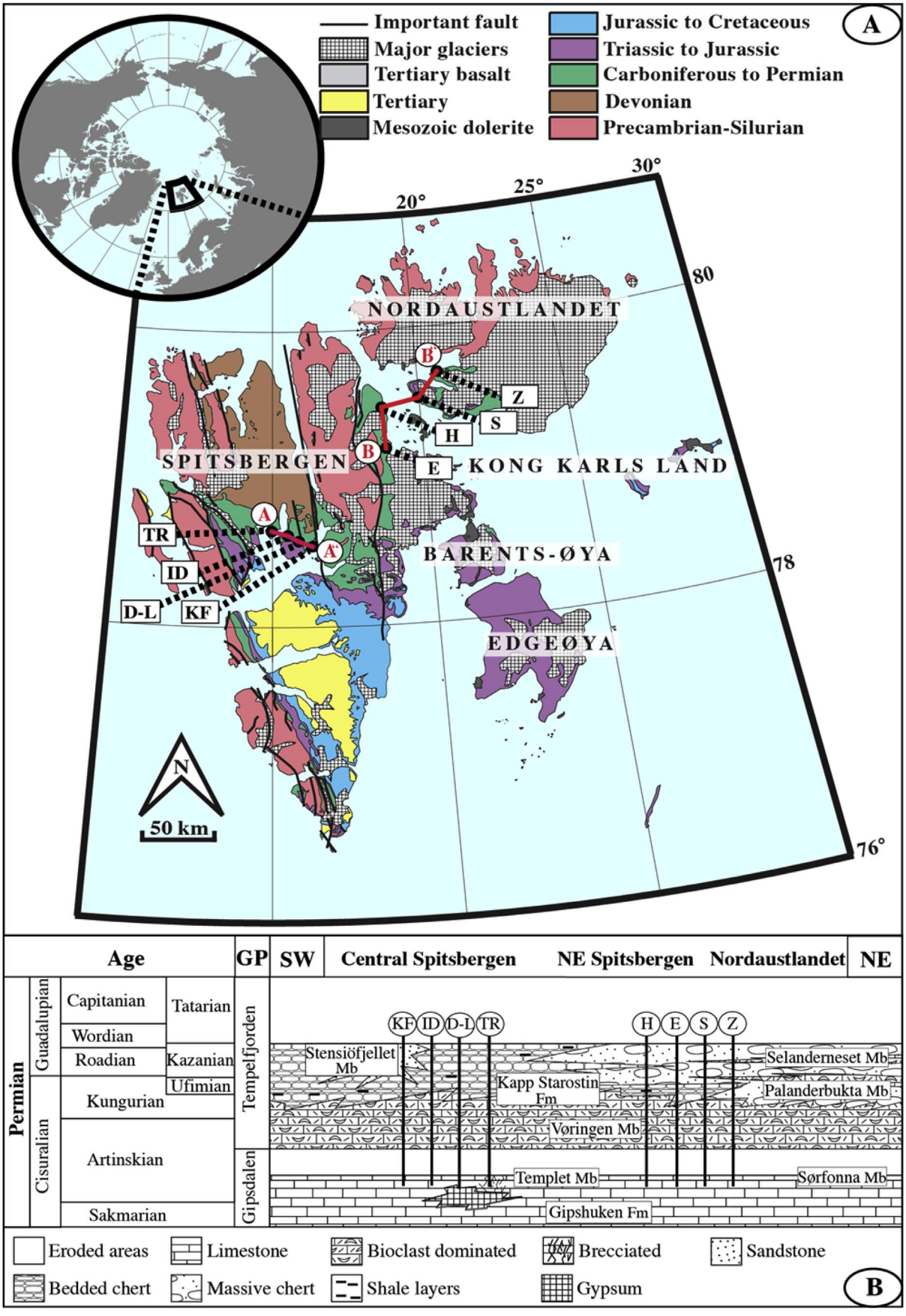

(caption on next page)

Fig. 1. A) Geological map of the Svalbard archipelago. Strata studied for this paper are of the Permian age indicated with the green shaded parts on the map (Dallmann et al., 1999). Sections location on Central Spitsbergen (Kapp Fleur de Lys (KF); Idodalen (ID); Tålmodryggen (TR): present study; and Dickson Land (D-L): Ehrenberg et al., 2001) and NE Svalbard (Eremitten (E); Hódbreen (H); Selanderneset (S); Zeipelfjella (Z): Blomeier et al., 2011, 2013) are indicated. A-A″ and B-B″ indicate cross-sections used for the geological profiles in Figs. 4 and 5. B) Chronostratigraphic framework and main lithologies in the Permian succession of Svalbard (adapted from Dallmann et al., 1999) with a schematic overview of the stratigraphic positions of the studied sections and formations. (For interpretation of the references to colour in this figure legend, the reader is referred to the Web version of this article.)

obtained from outcrops. These models can not only fill the gap between high-resolution outcrop observations and low-resolution seismic data, but can also answer questions related to the origin of the seismic reflectors (Bracco Gartner, 2000; Falivene et al., 2010; Janson et al., 2007; Kenter et al., 2001; Kleipool et al., 2015; Schwab et al., 2007; Zeller et al., 2015).

1D synthetic seismic traces provide the direct comparison of the seismic response and the associated rock properties. 2D synthetic seismic profiles resulting from a sequence stratigraphic framework allow for a comparison with real seismic data (Hodgetts and Howell, 2000). The usability of the seismic outcrop modelling is validated by a comparison with real seismic data of comparable sedimentary systems. This analogy can help to understand to what extent subsurface and outcrop are similar, and how much information from the outcrop can be used for reservoir models. (Bracco Gartner, 2000; Falivene et al., 2010; Jacquin et al., 1991; Ravenne and Vially, 1988; Schwab et al., 2007).

This study focuses on three selected outcrops, sections Kapp Fleur de Lys, Idodalen, and Tålmodryggen, on Spitsbergen (Svalbard Archipelago, Norway) (Fig. 1). The outcrops cover the Permian biosiliceous carbonate to carbonate succession of the Gipshuken and Kapp Starostin Formations representing two different carbonate factories. From bottom to top they are: (i) a tropical factory (T-factory, Schlager, 2005) with a photozoan microfacies association e.g., green algae and benthic foraminifera; and (ii) a cool and cold-water factory (C-factory, Schlager, 2005) with associated heterozoan biota, e.g., brachiopods, bryozoans, echinoderms, and siliceous sponges. The carbonates formed by the T-factory show a flat-topped platform geometry with a shallow-water lagoon and steep slopes. The carbonates associated with the C-factory lack platform rims and tend to form seaward sloping profiles in equilibrium with wave action, resulting in a ramp-type morphology with spiculitic mound structures.

The petrophysical properties, depositional setting and sequence stratigraphy of the investigated area have been studied in detail (Blomeier et al., 2011, 2013; Ehrenberg et al., 2001; Jafarian et al., 2017a,b) and were used as primary input for the synthetic seismic analysis. The seismic models were produced using multiple frequencies (25, 35, 50, 100, 200, and 400 Hz). The output is compared with the microfacies, rock property distribution and the general stratigraphic framework exposed in the outcrop. This comparison is used to examine the ability of seismic frequencies to resolve outcrop observations and will help to explain how much of the lithologic information ideally can be obtained from seismic data (Janson et al., 2007; Kleipool et al., 2017).

The biosiliceous and carbonate sediments researched are marked by a wide variability of petrophysical properties (porosity, density, and acoustic properties), which complicate seismic interpretations (Jafarian et al., 2017a). These deposits are reservoir rocks in various basins, e.g., the Permian Basin (West Texas; Montgomery, 1998) and the Finnmark Platform (Norwegian Barents Sea; Colpaert et al., 2007; Ehrenberg et al., 2001). Therefore, this study will be of benefit in understanding the seismic expression of the biosiliceous carbonate – carbonate succession and link the sedimentological and petrophysical properties retrieved from outcrop studies to seismic data in reservoir analogues.

2. Geological setting

During the Upper Palaeozoic, the Franklinian epicontinental shelf was situated at the northern rim of Pangea. It was arranged into a series of platforms and basins, e.g., Svalbard, the Finnmark Platform, and Stappen High (Barents Sea), the Wandel Sea Basin (eastern North Greenland), the Sverdrup Basin (Arctic Canada) and the Timan-Pechora Basin (Russia). This platform-basin configuration gradually moved from nearly low-latitude position at 25°N in the Upper Carboniferous to a more northern position at approximately 45°N in the Upper Permian (Golonka, 2002; Scotese and Langford, 1995).

Spitsbergen is the main island of the Svalbard archipelago (Fig. 1A) and shows a well-exposed upper Palaeozoic sedimentary succession comprising the Early Carboniferous to Early Permian Gipsdalen Group and the Early to Late Permian Tempelfjorden Group (Fig. 1B) (Nakrem et al., 1992).

The Templet Member is the top part of the Gipshuken Formation (upper formation of the Gipsdalen Group) in Central Spitsbergen and shows the deposition of evaporite/carbonate cycles indicating restricted, peritidal platform settings and sabkha (Dallmann et al., 1999). Lower Permian (Artinskian) sediments related to the regressive phase are observed in the Templet Member tops and are marked by intensely altered intraformational clasts embedded in fine-grained sediment or blocky sparite representing an exposure surface (Fig. 1B) (Blomeier et al., 2011; Ehrenberg et al., 2001; Groen, 2010).

The Tempelfjorden Group comprises the Kapp Starostin Formation in Central and NE Spitsbergen as well as Nordaustlandet (Fig. 1B). It starts with the Vøringen Member (except the Brøggerhalvøya) that is marked by heterozoan limestones (brachiopods, echinoderms, bryozoans) accumulating in cool-water conditions of a nearshore setting during a marine transgression (Blomeier et al., 2011, 2013). The member is succeeded by spiculitic cherts representing cold and deep-water environments, which are associated with a number of palaeogeographic (closure of the Ural Ocean) and palaeoceanographic variations (upwelling of cold, nutrient-rich deep waters) (Beauchamp, 1994; Blomeier et al., 2011, 2013; Stemmerik and Worsley, 1989).

In Central Spitsbergen, the upper part of the Kapp Starostin strata is described as the Stensiöfjellet Member which is composed of glauconitic sandstones, limestones and spiculitic cherts representing nearshore deposition (Fig. 1B) (Dallmann et al., 1999). The transition of the Stensiöfjellet deposits to the overlying Sassendalen Group (Triassic) is characterized by a rapid shift to marine siliciclastics (shales, siltstones and to a lesser extent sandstones) (Blomeier et al., 2011; Dallmann et al., 1999).

3. Methods

3.1. Input parameter

Previous work on Svalbard comprised detailed field and laboratory analyses to study the Templet strata and the Kapp Starostin successions (Blomeier et al., 2011, 2013; Ehrenberg et al., 2001; Jafarian et al., 2017a,b). Geological parameters such as microfacies characteristics, stratigraphic framework, and petrophysical properties (sonic velocity, porosity, and bulk density) were acquired from sections described during earlier studies. This information was used as input to construct a geological model (GM), an acoustic impedance model (AIM) and resulting 1D and 2D synthetic seismic models.

3.2. Geological framework

During fieldwork in Central Spitsbergen, three sections, Kapp Fleur de Lys (KF), Idodalen (ID), and Tålmodryggen (TR), have been measured (e.g., lithology, components, sedimentary structures, and colour) that range in thickness from 97 m to 139 m. Based on thermogravimetric analysis (TGA) and thin section analyses (texture and

composition) on 39 samples collected from the sections, nine different microfacies were distinguished covering a proximal and distal part of the depositional system. Individual samples were used to characterize the vertical microfacies distribution in three stratigraphic sections from Central Spitsbergen and provide a geological framework for 1D synthetic seismic logs.

The environmental microfacies interpretation was used to identify the relative water depth during deposition and to develop a sequence stratigraphic model for the measured sections. Based on the sedimentological observations (bed-scale to outcrop-scale) and sequence stratigraphic correlations, the microfacies distribution panel over Central Spitsbergen (section D-L: Ehrenberg et al., 2001; sections KF, ID, and TR: Jafarian et al., 2017b) and NE Svalbard outcrops (sections E, H, S, and Z: Blomeier et al., 2011, 2013) was established, which represents the geological model (GM).

The defined microfacies in the GM were vertically extrapolated to reach an equal height, thus filling the eroded zones of the upper portion of the sections. Without the extrapolation, some areas would remain unfilled and seismic artefacts could show up (Kleipool et al., 2017). This model was used during the 2D synthetic seismic modelling and allowed comparison with real seismic data (Hodgetts and Howell, 2000).

3.3. Acoustic impedance model (AIM)

In order to construct synthetic seismic logs and profiles of outcrops, it is important to understand the petrophysical characteristics of the individual microfacies. The product of compressional velocity (Vp) and bulk density (ρBulk) is the acoustic impedance (AI) which is the key property controlling the seismic response (Stafleu, 1994).

Velocity values were measured under realistic subsurface confining pressure (40 MPa: representing around 1,5 km depth) to ensure that the terminal velocity of each sample is reached (Bourbié et al., 1987). In the subsurface, rocks are saturated with brine in nearly all settings. The Gassmann fluid substitution (Gassmann, 1951) predicts saturated compressional wave velocities. It assumes that shear moduli remain constant during fluid substitutions while many carbonate rocks show shear weakening or shear strengthening (Adam et al., 2006; Baechle et al., 2005). Due to this limitation of the Gassmann theory we used dry P-wave velocities. Besides that, due to generally low porosity, fluids or gasses which can fill intergranular space within sedimentary rocks are excluded. Thus, the dominant intergranular space is assigned to cement or micrite.

This biosiliceous – carbonate depositional system is marked by a wide variability in microfacies types. Hence, the average values of the dry P-wave velocity (at 40 MPa) and dry bulk density (ρBulk) of each defined microfacies were multiplied to calculate acoustic impedances (Eq. (1)).

$$AI = Vp * \rho Bulk \tag{1}$$

Calculated averages of porosity, dry bulk density (ρBulk), dry P-wave velocity, and the acoustic impedance of each microfacies were assigned to the individual microfacies bodies in the GM to show the spatial distribution of petrophysical properties within sections. In some microfacies (MFTs-1, 2 and 6), only one sample was accessible. The acoustic impedance model (AIM) was used to create 2D synthetic seismic profiles.

To construct 1D synthetic seismic logs, vertical microfacies transitions in the sections (KF, ID, and TR) were used. The acoustic impedance values of each sample of the individual microfacies were calculated and assigned to the corresponding layers in the sections. Sampling gaps in the sections were populated with calculated impedance values based on their microfacies characteristics (colour, texture, grain size, components) provided by the detailed stratigraphic field logs.

3.4. Synthetic seismic modelling

Vertical changes in acoustic impedance are used to calculate the reflection coefficients (R) (Eq. (2)) (Stafleu et al., 1994). To create a link between the rock properties and real analogue seismic data, the vertical reflection coefficients (R) were convoluted to seismic traces using a zero-phase Ricker wavelet (Ricker, 1953) at various frequencies (25, 35, 50, 100, 200, and 400 Hz). The output was imported into SeisLab, an application written in MATLAB® (MathWorks, Natick, Massachusetts, USA) visualizing seismic models. To generate a continuous 2D seismic profile a series of 250 shotpoints are interpolated, the 1D synthetic seismic log is created from a single shotpoint.

$$R = \frac{AI2 - AI1}{AI2 + AI1} \tag{2}$$

Zero-phase wavelets were selected because they have a higher resolution than minimum phase wavelets and the peaks of Ricker wavelets are centred at the reflecting boundaries (Schoenberger, 1974).

In 1D and 2D seismic models, the increment in acoustic impedance is represented by hard-kick signals (positive peak; red) and the decrease in acoustic impedance is characterized by soft-kick signals (negative peak; blue).

The vertical resolution of the high-frequency seismic signal was approximated at 3.5 m (quarter wavelength criterion assuming a 400 Hz peak frequency and 5500 m/s average velocity; Eq. (3)), which decreased to about 55 m when lowering the wavelet frequency to 25 Hz. The 25–50 Hz frequencies are commonly used in E&P industry, since they may reach potential hydrocarbon depths (Stafleu et al., 1994). The low-frequency synthetic seismic models are used for comparison with subsurface seismic data. The high-frequency wavelets (100–400 Hz) do not reach that depth but emphasize which features of the depositional setting such as microfacies distribution and geometry were overlooked with decreasing wavelet frequency.

$$Wavelength\ (\lambda) = \frac{Velocity\ \left(\frac{m}{s}\right)}{Frequency\ (Hz)} \tag{3}$$

4. Results

4.1. Microfacies analyses

The studied succession covers a large variety of microfacies types. Nine microfacies types were recognized according to their lithology, texture, grain size, main components and consequently their depositional environment (Fig. 2). The following microfacies types were defined: MFT-1: Sandstones, MFT-2: Clay-to siltstones, MFT-3: Spiculitic massive cherts, MFT-4: Spiculitic bedded cherts, MFT-5: Coarse-grained, bryozoan limestones, MFT-6: Lithoclastic rudstones (carbonate breccias), MFT-7: Fine-grained, mixed-bioclastic limestones, MFT-8: Microbial limestones, MFT-9: Coarse-grained, brachiopod limestones. Table 1 provides more detailed information of the individual microfacies types, e.g., porosity, mineralogy, acoustic impedance. An extensive description of the microfacies can be found in Jafarian et al. (2017b).

4.2. Sections

4.2.1. Kapp Fleur de Lys section (Section KF)

At this location (Figs. 1 and 3), the Templet Member is marked by an alternation of microbial limestones and mudstones (MFT-8) that are succeeded by lithoclastic rudstones (carbonate breccias; MFT-6). It shows an increase in thickness when moving from Kapp Fleur de Lys section to Tålmodryggen section (Fig. 3). The contact of the Templet and the overlying Vøringen Members is not exposed (Groen, 2010; Jafarian et al., 2017b). The succeeding Vøringen Member comprises

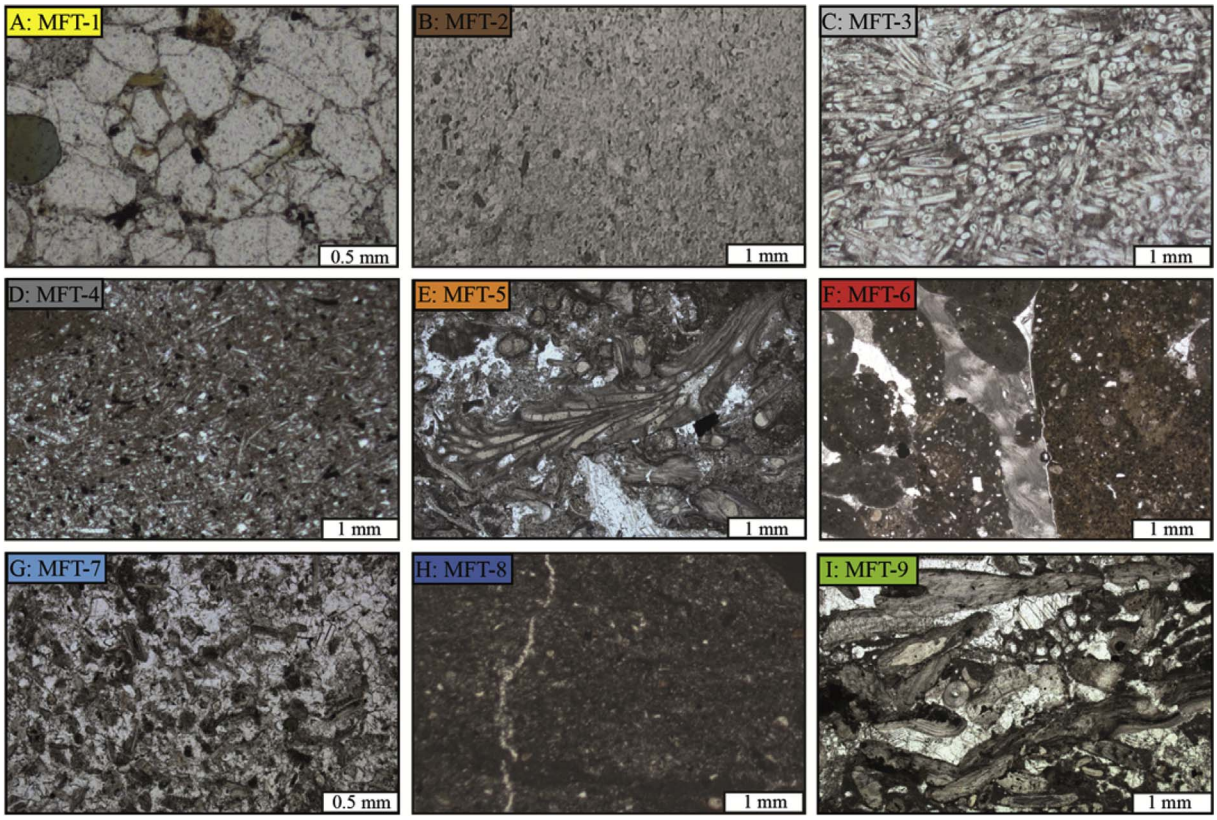

Fig. 2. Thin section photographs of each distinguished microfacies: A: MFT-1, Sandstones (Sk-1.41.1); B: MFT-2, Clay-to siltstones (FE-1.7.2); C: MFT-3, Spiculitic massive cherts (TR-1.62.1a); D: MFT-4, Spiculitic bedded cherts (TR-1.18.1); E: MFT-5, Coarse-grained, bryozoan limestones (ID-1.26.4); F: MFT-6, Lithoclastic rudstones (carbonate breccias) (TR-1.19.1); G: MFT-7, Fine-grained, mixed-bioclastic limestones (TR-1.18.1); H: MFT-8, Microbial limestones (ID-1.3.1); and I: MFT-9, Coarse-grained, brachiopod limestones (KF-1.9.1).

silicified, bioclastic limestones (MFTs-7 and 9), which show a fining-upward trend. A monotonous series of bedded and massive cherts (MFTs-3 and 4) with claystone partings (MFT-2) characterizes the Kapp Starostin Formation. The uppermost part of this section shows a succession of chert units (MFTs-3 and 4) grading into silicified, bioclastic limestones (MFT-9) and glauconite-rich sandstones (MFT-1) constituting the Stensiöfjellet Member.

4.2.2. Idodalen section (Section ID) and Tålmodryggen section (Section TR)

In sections ID and TR, the deposits of the Templet and Vøringen Members are lithological analogous to those outcropping in section KF (Figs. 1 and 3). However, in section TR, the Vøringen Member starts with a basal limestone breccia (MFT-6), which is absent in sections KF and ID (Fig. 3). This basal part is overlain by bioclastic cherty limestones (MFTs-7 and 9) and sandy horizons (MFT-1). In both localities (sections ID and TR), the deposits of the Kapp Starostin Formation continue with chert units (MFTs-3 and 4) and dark claystone horizons (MFT-2). The succession gradually shifts into silicified, heterozoan carbonates (MFT-5) which are less developed within section ID and not exposed at section KF.

4.3. Sequence stratigraphy

Based on the interpretations of depositional environments, the herein-defined microfacies are arranged in cyclic patterns developed by fluctuations of relative sea level (Fig. 3).

The Early to Late Permian (Artinskian to Kazanian) biosiliceous – carbonate succession on Spitsbergen shows a second-order cycle with a duration exceeding twenty Myr (Nichols, 1999), which can be subdivided into five third-order sequences (Jafarian et al., 2017b) (Fig. 3). The third-order parasequences (S0, S1, S2, S3, and S4) are packages of beds that demonstrate a progradational pattern with a thickness of several tens of meters and a range of one to ten Myr (Nichols, 1999). The boundaries of the parasequences (PSB1, PSB2, and PSB3) are marked by an abrupt rise in relative sea level followed by a sudden shift from shallow (e.g., carbonates and sandstones) to deep marine microfacies (e.g., claystones and cherts). The top of the shallowest unit is interpreted as the parasequence boundary. However, SB shows the boundary between the Templet (S0) and Vøringen (S1) Members, which is characterized by the lowest base level in the studied area and representing periods of subaerial exposure. This surface is interpreted as the sequence boundary and indicates a hiatus. PSB1 separates the Vøringen Member from the Kapp Starostin Formation (S2) and, PSB2 and PSB3 are positioned between the shallowest and deepest units within the Kapp Starostin strata.

The following parasequences were defined:

- (S0): This cycle comprises Templet Member developing in a marginal marine environment. It shows a progradational pattern, which is marked by microbial limestones (MFT-8) topped by carbonate breccias (MFT-6) and *Microcodium* bearing sediments suggesting periods of subaerial exposure (Fig. 3). Hence, the upper part of this regressive cycle is interpreted as an unconformity boundary (SB).
- (S1): This parasequence contains the Vøringen Member. At section ID (not exposed in section KF) this cycle is started with claystone horizon (MFT-2) that represents a substantial relative rise in sea level (Fig. 3). In section TR, heavily altered extraclasts (MFT-6) of older strata within the lower part of the Vøringen Member, indicate erosion of earlier deposits through high wave energy (during transgression) in the shallow-water area. The shallowing-upward trend is marked by coarse-grained, bioclastic limestones (MFT-9) (Blomeier et al., 2011; Groen, 2010). The occurrence of fine-grained, heterozoan limestones (MFT-7) at the top of this succession

Table 1
Petrophysical properties and Textural characteristics, occurrence, and environmental reconstruction of the microfacies types (MFTs) from Spitsbergen.

MFT-Number	MFT-Name	Carbonate range (%)	Porosity range (%)	Bulk density range (g/cc)	Vp (40MPa) (km/s)	Acoustic impedance range (Nsm^{-3})	Dominant pore type	Texture	Components	Occurrence	Depositional environments
MFT-1	Sandstones	0.40	11.8	2.35	4.46	10.49	Reference	Sandstone	Well-sorted, edge-rounded to rounded, sand-sized quartz grains, less than 5% glauconite minerals	Kapp Starostin Fm.	Represent alluvial to shore face conditions of the inner shelf
MFT-2	Clay- to siltstones	6.80	1.0	2.59	5.39	14.00	Crack	Clay- to siltstone	Components are not clear recognizable due to obliteration of primarily origin	Kapp Starostin Fm.	Reflect quiet environments, typically for the deep marine area of the outer ramp
MFT-3	Spiculitic massive cherts	6.5–25.9	0.7–20.7	2.08–2.61	3.76–5.70	7.83–14.83	Crack	Packstone to wackestone	Abundant megaspicules, arenitic to ruditic skeletal fragments (often heterozoan). Sediments are intensively silicified	Kapp Starostin Fm.	Form around and below the SWWB
MFT-4	Spiculitic bedded cherts	4.8–45.2	0.7–2.6	2.48–2.64	4.55–5.85	11.30–15.48	Crack	Packstone to wackestone	Abundance microspicules and burrows in micritic matrix. The deposits are affected by silicification	Kapp Starostin Fm.	Form in quiet water, low-energy conditions below the SWWB
MFT-5	Coarse-grained, bryozoan limestones	42.1–87.3	0.4–1.7	2.63–2.68	5.54–5.79	14.61–15.40	Crack	Floatstone to rudstone	Poorly sorted debris of bryozoans, echinoderms, occasional brachiopods and spicules of sponge. Matrix is composed of micrite/microsparite. Sparry-filled inter- and intraparticle voids present	Kapp Starostin Fm.	Form in distal mid ramp around the SWWB
MFT-6	Lithoclastic rudstones (carbonate breccias)	76.1	1.3	2.70	5.44	14.70	Reference	Rudstone	Abundant angular to well-rounded intraformational clasts embedded in micritic/microsparitic matrix. Locally blocky or sytaxial sparite cemens are present	Templet Mb., Vøringen Mb.	Within sabkha environments, the former deposits are influenced by erosion, reworking and redeposition in diverse degrees
MFT-7	Fine-grained, mixed-bioclastic limestones	37.9–97.6	0.5–5.9	2.50–2.69	4.48–6.16	11.50–16.64	Crack	Grainstone	Mainly fine to medium brachiopod shell debris and sometimes sponge spicules are cemented by blocky sparite	Vøringen Mb.	Form in agitated water conditions around the FWWB
MFT-8	Microbial limestones	82.1–88.1	1.4–5.3	2.57–2.68	4.99–5.59	12.80–14.70	Crack	Bindstone	Abundant Algal mats, dense micritic peloids and sand-sized, quartz grains in micritic matrix	Templet Mb.	Reflect marginal-marine, tidal flats of a warm-water carbonate platform
MFT-9	Coarse-grained, brachiopod limestones	87.3–93.1	1.1–2.5	2.63–2.66	5.36-5.68	14.17–14.95	Crack	Rudstone	Abundant coarse-grained, well to poorly sorted, thick-shelled brachiopods, rare debris of bivalves, gastropods, trepostome bryozoans and echinoderms. Components mainly are cemented by sparite	Vøringen Mb.	Reflect high-energy, periodic storm events, during which the skeletal material was reworked and accumulated across the inner ramp (above FWWB)

might record a renewed deepening of the depositional environment at the transition into the overlying parasequence.

- (S2, S3, and S4): Cycles S2, S3 and S4 in the Kapp Starostin Formation show a similar microfacies arrangement, from basal claystone horizon and bedded cherts (MFTs-2 and 4) to massive chert (MFT- 3). These deposits locally followed by a coarsening and shallowing-upward trend into bioclastic limestones (MFT-5) (Fig. 3).

Lower-order sea-level variations (fourth and fifth-order cycles) or high-energy storms locally disturb parasequences (S2, S3, and S4) and subdivide them into a number of temporally shoaling-upward cycles (Jafarian et al., 2017b) (Fig. 3).

4.4. Geological model (GM)

Lateral modelling of sedimentary facies provides a better understanding of the microfacies variability during sedimentation. Based on the microfacies distribution and defined sequence/parasequence boundaries, third-order sequences and associated microfacies in Central Spitsbergen and NE Svalbard are laterally correlated to produce a geological model (GM) (Figs. 4 and 5) (Jafarian et al., 2017b). The latter shows that section TR (Central Spitsbergen) is positioned in a proximal shallow-water setting marking by a higher input of extraclasts and sand content in the Vøringen Member and a greater portion of shallow-water microfacies (limestones) in the Kapp Starostin Formation (Fig. 4). Towards section KF, limestones gradually become thinner while deep-water bedded cherts (MFT-4) increase in thickness.

There is an overall limited lateral microfacies variation, and comparable sedimentation patterns occur along NE Svalbard up to Central Spitsbergen (Figs. 4 and 5). The geological models (GM) suggest that NE Svalbard is positioned at a low accommodation locality as shown by the thinner sequences and shallower microfacies (massive cherts, sandstones, and bioclastic limestones) of the Kapp Starostin Formation. However, the Vøringen Member shows deeper-water sedimentation (bryozoan limestones) in this area compared with Central Spitsbergen (Figs. 4 and 5).

4.5. Petrophysical properties

The 39 samples that were used for modelling represent a wide range of petrophysical properties (Table 1; Fig. 6).

The mineralogical composition of the sediments covers a broad range of carbonate contents from 0.4% to 97.6%. The carbonate content decreases from the Templet Member to the Kapp Starostin Formation

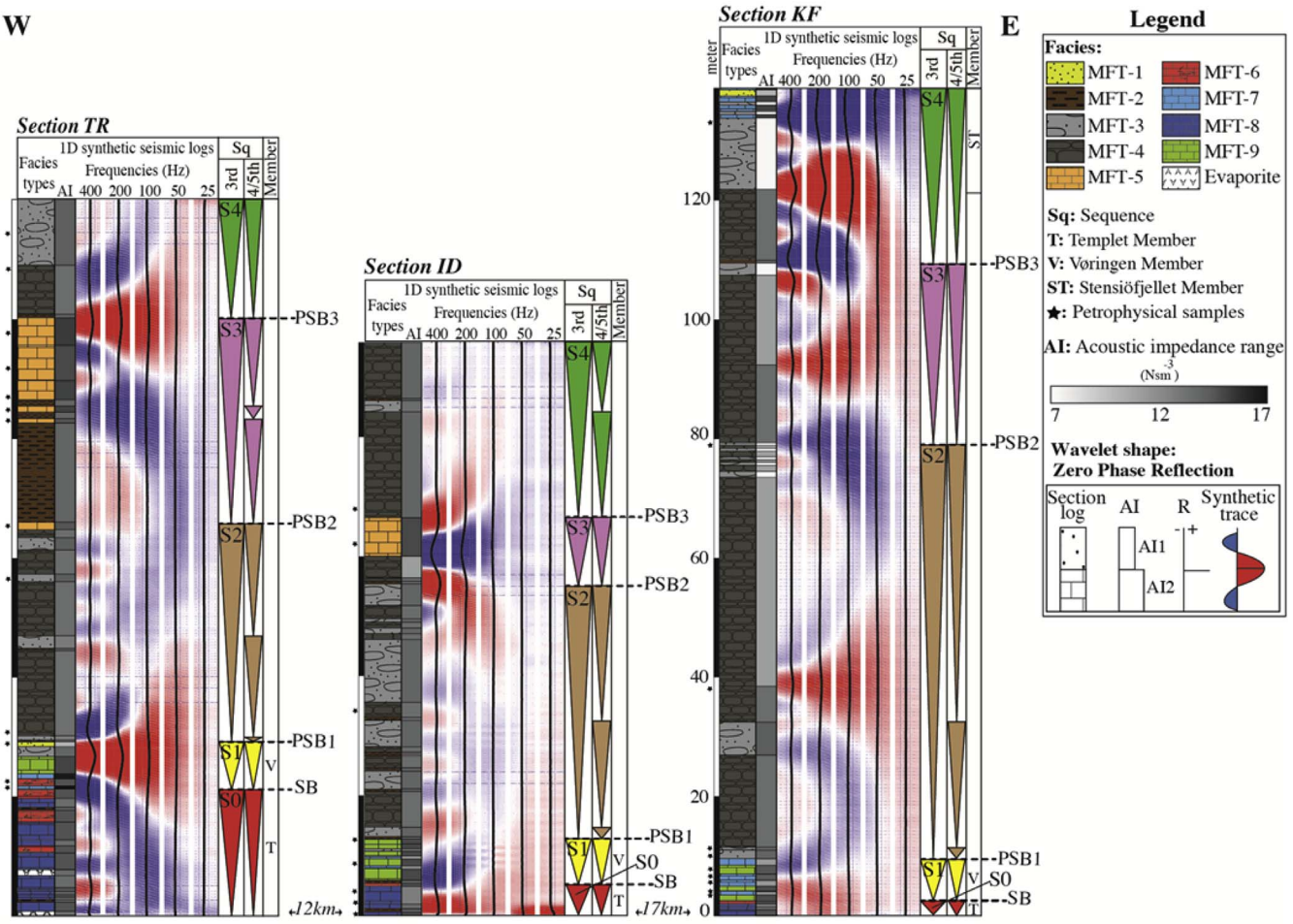

Fig. 3. A detailed overview of sedimentological sections (TR, ID, and KF) in Central Spitsbergen showing thickness, main lithology, depositional cycles (third, fourth/fifth-orders) and sequence/parasequence boundaries (SB, PSB1, PSB2, and PSB3). Besides, acoustic impedance variations and 1D synthetic seismic traces are added. A Ricker wavelet (Ricker, 1953) is used with an array of different frequencies (25, 50, 100, 200, and 400 Hz). The red colours are positive signals (hard-kick) and blue colours are negative signals (soft-kick). (For interpretation of the references to colour in this figure legend, the reader is referred to the Web version of this article.)

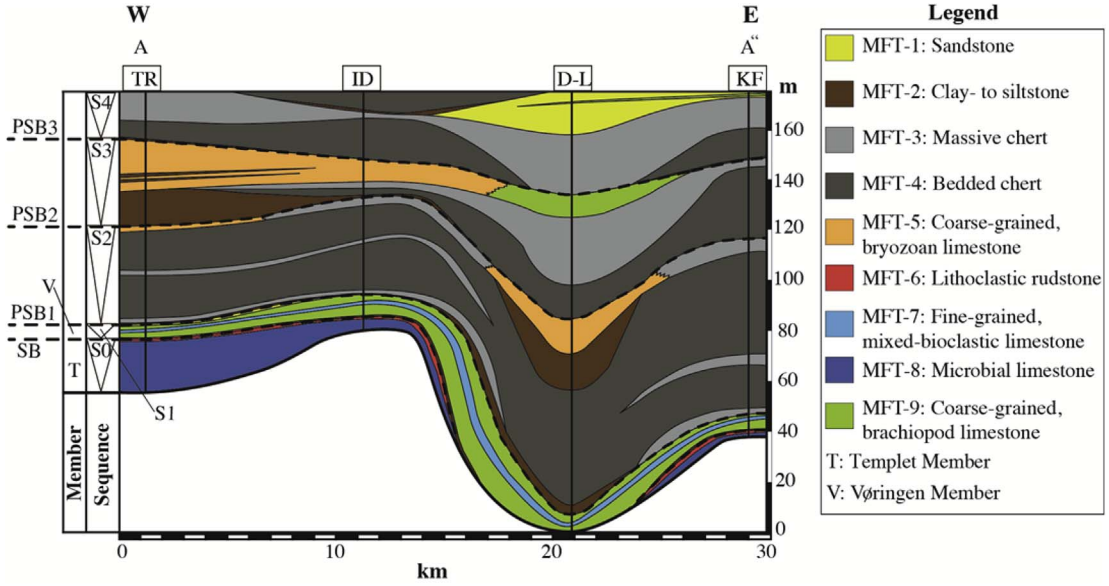

Fig. 4. The geological model of Central Spitsbergen based on the sequence stratigraphy correlation showing lateral microfacies changes. Section locations (TR, ID, D-L, and KF), third-order sequences (S0, S1, S2, S3, and S4), and sequence/parasequence boundaries (SB, PSB1, PSB2, and PSB3) are added.

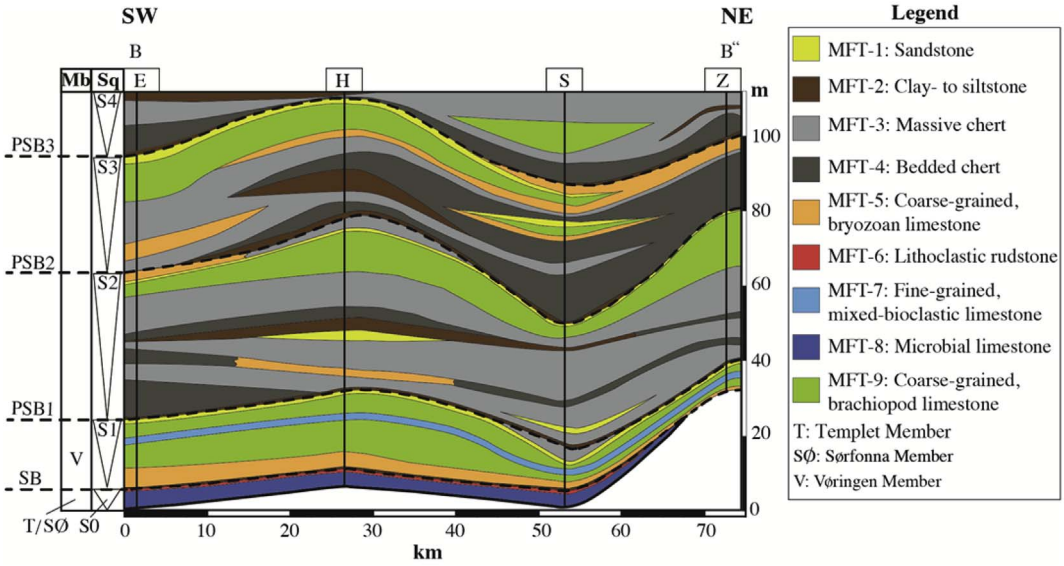

Fig. 5. The geological model of NE Svalbard based on the sequence stratigraphy correlation showing lateral microfacies changes. Section locations (E, H, S, and Z), third-order sequences (S0, S1, S2, S3, and S4), and sequence/parasequence boundaries (SB, PSB1, PSB2, and PSB3) are added.

while the biogenic silica (spicules) content increases (Table 1).

Each microfacies type is characterized by different amounts of porosity and an almost certain mineralogical composition. Porosity values fall between 0.4% and 5.9% except for two porous samples with 11.8% (sandstones) and 20.7% (spiculitic massive cherts) porosity. Since variability of porosity within the studied samples is generally low, the porosity has been considered constant (average) for a given microfacies in the petrophysical input models. Thus, lateral and vertical porosity changes within each microfacies body are not incorporated in the 2D models while they are considered as 1D synthetic seismic logs.

The bulk density distribution shows that the lowest bulk density value 2.08 g/cc occurs in the spiculitic massive cherts microfacies (MFT-3), and lithoclastic rudstones microfacies (MFT-6) have the highest bulk density value, 2.70 g/cc (Table 1; Fig. 6A). At a pressure of 40 MPa, compressional velocities of the mixed facies vary from 3.76 to 6.16 km/s. The acoustic impedance values range between 7.83 and 16.64 Nsm^{-3} and are generally higher in the carbonate-rich microfacies (MFTs- 5 to 9) (Table 1; Fig. 6B).

Petrophysical input models (Figs. 7 and 8) illustrate that the highest average porosity (11.8%) and lowest average bulk density (2.35 g/cc) is covered by sandstone microfacies. Hence the lowest average velocity (4.46 km/s) and acoustic impedance (10.49 Nsm^{-3}) occurs in this microfacies. The highest averages of Vp (5.68 km/s) and acoustic impedance (15.06 Nsm^{-3}) are measured in the coarse-grained, bryozoan limestone microfacies (MFT-5) in combination with the lowest average porosity (0.99%).

4.6. Synthetic seismic logs (1D)

The observed outcrop microfacies distributions on Central Spitsbergen have been translated into synthetic seismic logs at multiple frequencies, e.g., 25, 50, 100, 200 and 400 Hz (Fig. 3).

4.6.1. Sequence/parasequence boundary

In sections TR and ID, the sequence boundary (SB) between the Templet and Vøringen Members is marked by a soft-kick signal in the 200–400 Hz logs (Fig. 3). In a distal realm (section KF), this boundary is not reflected within the synthetic seismograms since the thickness of the Templet Member falls below seismic resolution.

The 200 and 400 Hz logs show that PSB1 in section KF represents the shift from relatively high-porous, fine-grained, mixed-bioclastic limestones (MFT-7) of the Vøringen Member to the overlying silicified cherts (MFT- 3) of the Kapp Starostin Formation (Fig. 3). This transition is reflected as a low-amplitude soft-kick signal. In section TR, the upper

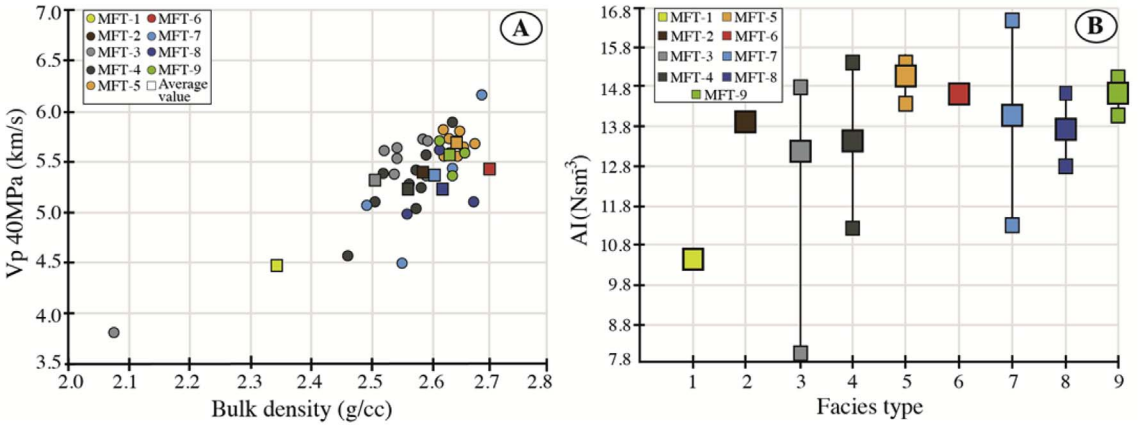

Fig. 6. A) Cross plot of measured dry P-wave velocity and bulk density for each measured sample coded by microfacies. Circle symbols indicate the measured value of one sample for each microfacies, whereas square symbols indicate the average values for each microfacies. B) The acoustic impedance domains are arranged by microfacies type (MFT). The small squares indicate the maximum and minimum values measured; the large square relates to the average value of the specific MFT.

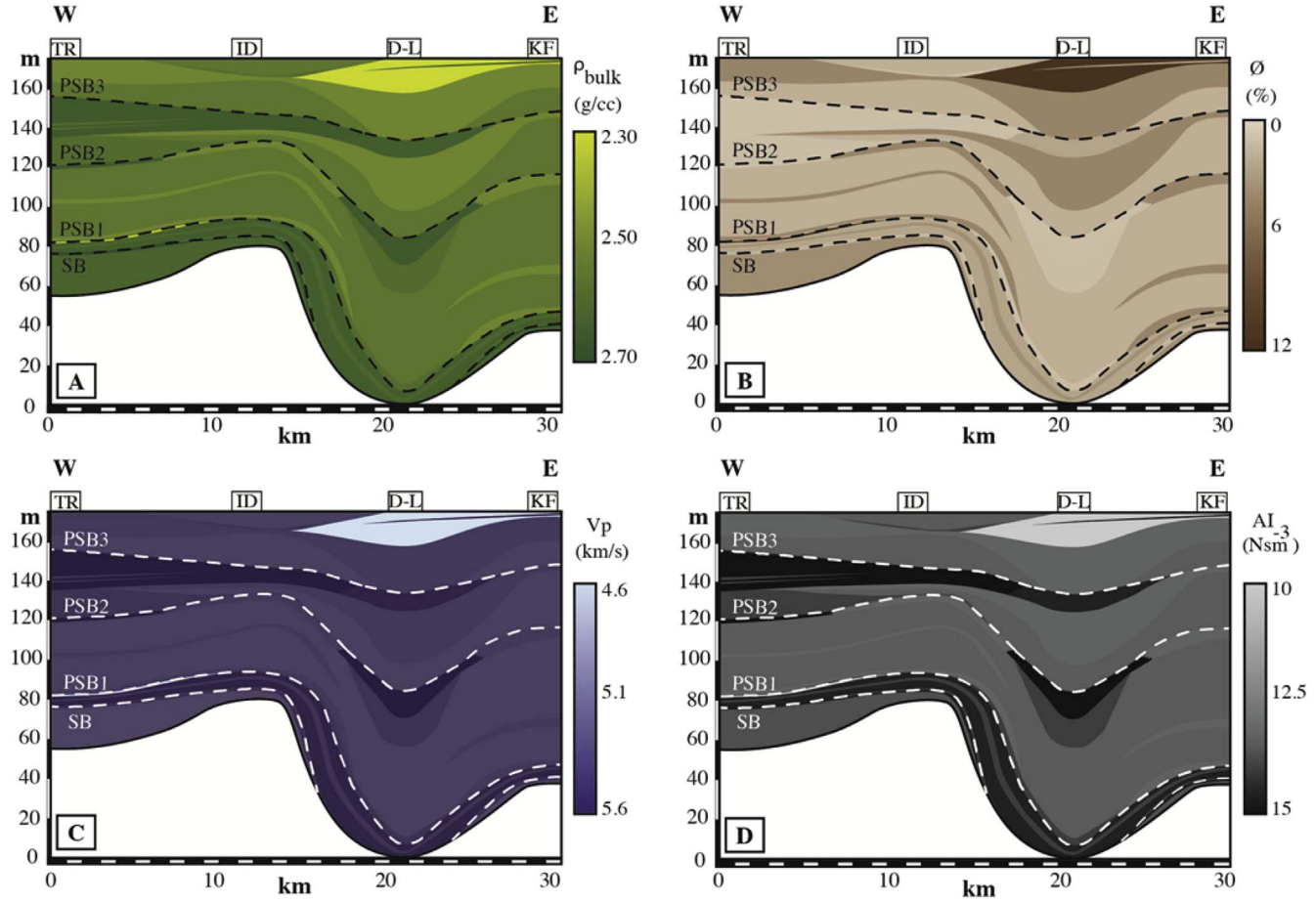

Fig. 7. Petrophysical input models: the distribution of bulk densities (A), porosities (B), pressure wave velocities (C) and the calculated acoustic impedances (D) are superimposed on the geological models of Central Spitsbergen. Sections location and sequence/parasequence boundaries (SB, PSB1, PSB2, and PSB3) are added.

part of the Vøringen Member is marked by massive cherts, which are lithologically similar to the overlying Kapp Starostin strata (Fig. 3). These top chert units show a different mineralogical composition compared with the lower carbonate sediments (MFT-9). The interface between them is reflected as a pronounced hard-kick signal. Therefore, facies similarity of the top of the Vøringen Member and the overlying Kapp Starostin strata cause a downward shift in the position of PSB1 within the synthetic seismograms. In section ID, the microfacies transition within the Vøringen Member frequently changes on a meter or sub-meter scale resulting in destructive interfering waves.

The 200 and 400 Hz logs display that in section KF, the gradual shift from massive cherts to bedded cherts across PSB2 is expressed as a soft-kick signal (Fig. 3). This is in contrast to the pronounced hard-kick signal at this boundary in section ID. PSB2 in section TR is marked by a sharp transition from bryozoan limestones to overlying shales, expected to show a hard-kick signal at this interface (Fig. 3). However, this transition is obliterated in the seismic seismograms, which might be due to the limited thickness of carbonate layer falling below seismic detectability.

In section KF, PSB3 separates deep-water shale and bedded cherts from porous massive cherts of the underlying cycle. This transition is expressed as a pronounced soft-kick signal in the 100–400 Hz logs (Fig. 3). In contrast to section KF, PSB3 shows a distinct hard-kick signal in sections TR and ID representing carbonates overlain by shale and spiculitic cherts (Fig. 3).

4.7. Synthetic seismic profiles (2D)

4.7.1. Sequence/parasequence boundary

In Central Spitsbergen and NE Svalbard, the lithoclastic rudstone (MFT-6) and shale layer (MFT-2) interface marking the sequence boundary (SB), falls below seismic detectability. Hence, SB shows the transition from the microbial limestones (MFT- 8) of the Templet Member to the coarse-grained, heterozoan carbonates (MFTs- 5 and 9) of the Vøringen Member and is reflected as a low-amplitude soft-kick signal in the 400 Hz profiles (Figs. 9 and 10).

PSB1 displays the transition of carbonate (Vøringen Member) to shale and spiculitic chert (Kapp Starostin Formation) and is detected as a continuous hard-kick signal (100–400 Hz profiles) along NE Svalbard up to Central Spitsbergen (Figs. 9 and 10). However, at the location of section S in NE Svalbard (Fig. 5), the occurrence of massive cherts at the top of the Vøringen strata record a renewed deepening of the sedimentary environment at the transition into the subsequent parasequence. This shift towards the overlying shale and chert layers is reflected as a soft-kick signal in the 400 Hz model (Fig. 10). The alternating layers of sandstone and shale across the PSB1 fall below the seismic detectability.

The high-frequency profiles (200 and 400 Hz) show that in both areas (NE Svalbard and Central Spitsbergen), PSB2 and PSB3 generally represent the interface between the carbonates on top of the shallowing-upward cycle and the overlying deep-water cherts. PSB2 and PSB3 are expressed as strong positive seismic signals (Figs. 9 and 10). The facies change over, e.g., sandstone to shale, across these boundaries thins below seismic resolution.

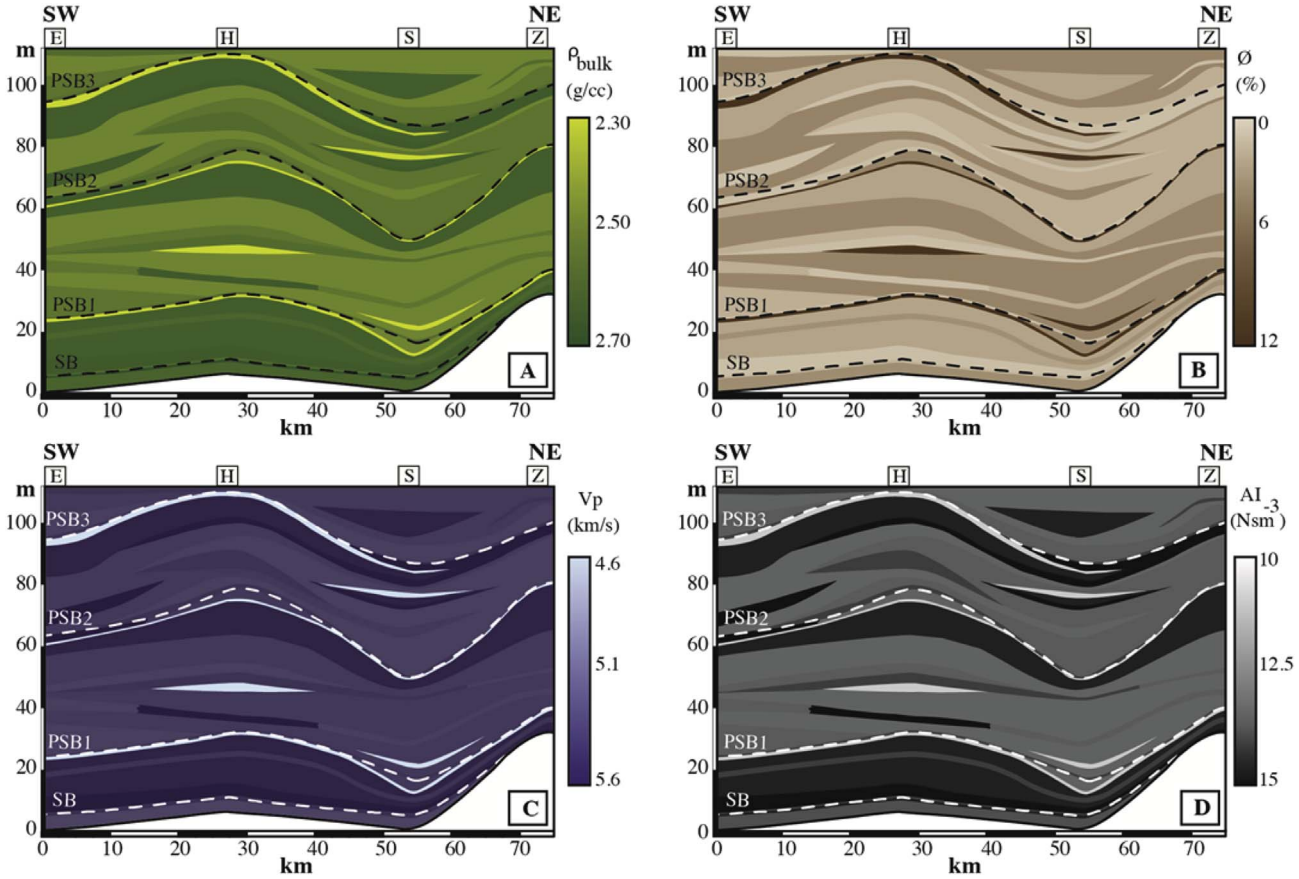

Fig. 8. Petrophysical input models: the distribution of bulk densities (A), porosities (B), pressure wave velocities (C) and the calculated acoustic impedances (D) are superimposed on the geological models of NE Svalbard. Sections location and sequence/parasequence boundaries (SB, PSB1, PSB2, and PSB3) are added.

5. Discussion

5.1. Interpretation of the synthetic seismic profiles

5.1.1. Structural style and morphology

The shape of the seismic reflectors follows the antecedent topography of the studied areas (Figs. 9 and 10). Anticline and syncline shapes can be recognized from the seismic reflectors, which imply thickness variations of the Kapp Starostin successions. During the Permian, no main tectonic movement has been documented on Svalbard. Differences in accommodation space most likely resulted from the distribution and reactivation of pre-existing structural elements, and eustatic sea-level fluctuations (Blomeier et al., 2013; Ehrenberg et al., 2001). The amplitude strength of seismic reflectors varies laterally emphasizing lateral changes in microfacies (Figs. 9 and 10). For example, at PSB2 in Central Spitsbergen, carbonates shift into massive cherts frequently (Figs. 4 and 9). Moreover, destructive interference patterns as a result of wedge-shaped sediments with microfacies alternating on a meter or sub-meter scale and microfacies pinch outs, cause a decline of amplitude reflectors and discontinuity of them in the studied areas. Continuity of seismic reflections is closely related to continuity of bedding. Seismograms generated with the low-frequency wavelets (25–100 Hz) do not show any detailed depositional geometries such as these microfacies pinch-outs and sediment wedges (Figs. 9 and 10). This holds for NE Svalbard in particular.

5.1.2. Sequence/parasequence boundary

Since sequence/parasequence boundaries are marked by a sudden shift from shallowest to deepest microfacies associated with high petrophysical contrasts, high-amplitude seismic reflectors are expected to occur at these transitions.

In the studied areas, the profound shift in carbonate producers from T-factory (Templet Member) to C-factory (Vøringen Member), see Table 2, has been associated with large-scale climatic, paleoceanographic and paleogeographic changes linked to the northwards drift of Pangea (Beauchamp, 1994; Beauchamp and Baud, 2002; Beauchamp and Grasby, 2012; Blomeier et al., 2011; Reid et al., 2007). Based on geological models, this carbonate switchover marks the sequence boundary (SB), which is reflected as a low-amplitude soft-kick signal (Figs. 3, 9 and 10).

Stafleu et al. (1994) demonstrated that the acoustic properties of tight limestones of the Vercors (France) might be controlled by grain-size and texture. In the studied synthetic seismic models, the low-amplitude, negative reflectors at SB can be explained by textural differences in carbonates resulting from depositional and diagenetic alterations (Table 2). The carbonate content of the micrite-supported sediments from the T-factory varies between 76.1% and 88.1%. These values largely correspond to the fraction of micrite filled interparticle space (MFTs-6 and 8). Sediments produced within the C-factory, on the other hand, are grain-supported. The wide range of carbonate content (37.9%–97.6%) is related to the type of grains and associated post-depositional processes. Diagenetic modifications such as cementation and recrystallization can change the pore network and texture of sedimentary rocks and to the associated acoustic impedance (Fournier and Borgomano, 2007; Jafarian et al., 2017a). In the investigated areas, bioclastic-dominated limestones associated with the C-factory (S1), which are affected by cementation and chertification, show higher acoustic velocities and impedances compared to the mud-dominated limestones formed by the T-factory (S0) (Jafarian et al., 2017a). The increase in acoustic properties can be explained by the framework of interlocking crystals that were formed during diagenetic processes. These rock modifications may result in higher rock rigidity and lower

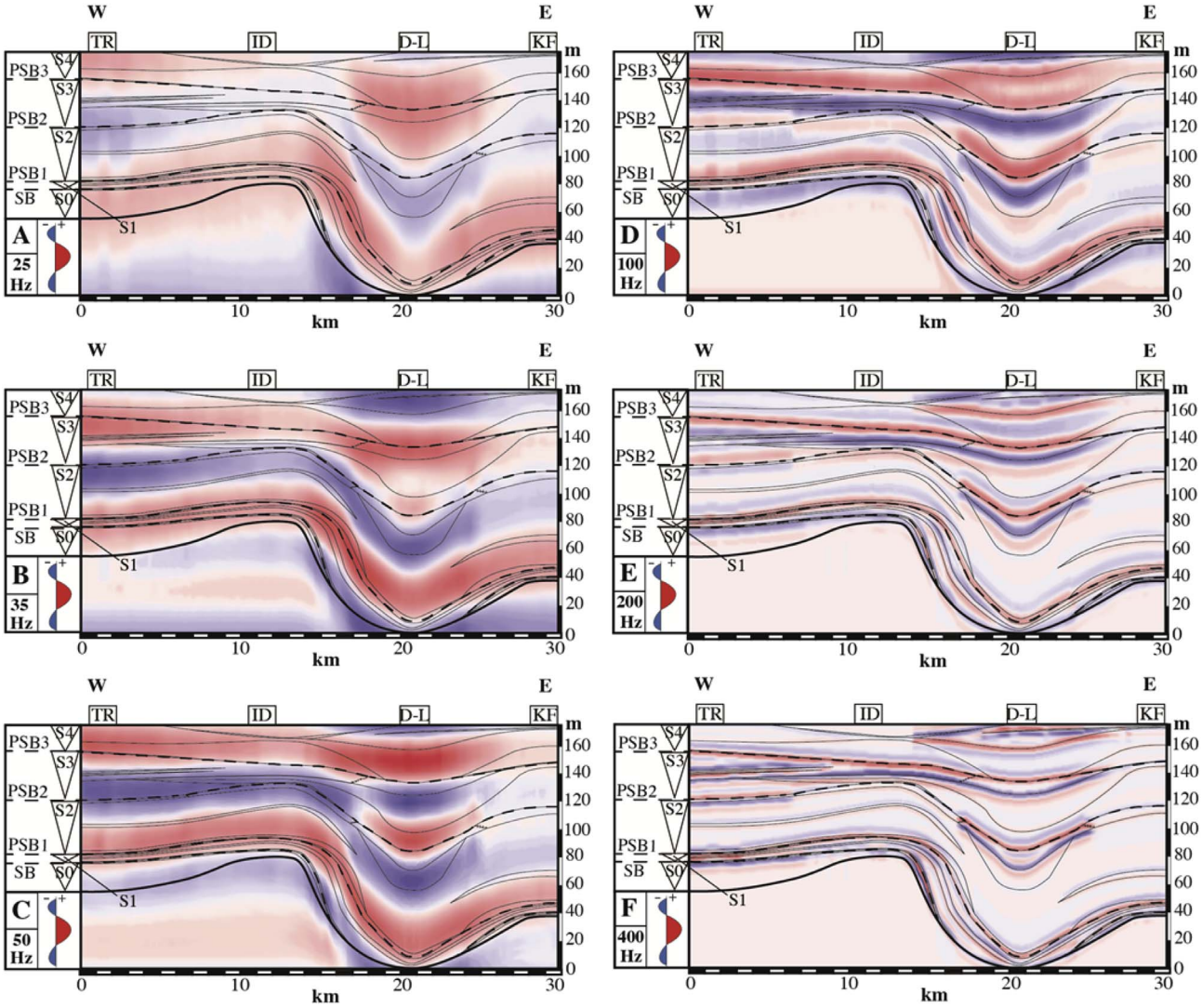

Fig. 9. Synthetic seismic profile at multiple frequencies (A: 25 Hz, B: 35 Hz, C: 50 Hz, D: 100 Hz, E: 200 Hz, F: 400 Hz) of Central Spitsbergen. Acoustic impedance values were used to calculate the reflection coefficients between the individual unit interfaces. Ricker wavelet (Ricker, 1953) was used for convolution to generate a synthetic seismic profile. The red colours are positive signals (hard-kick) and blue colours are negative signals (soft-kick). Sections location, microfacies transitions, defined third-order sequences (S0, S1, S2, S3, and S4) and sequence/parasequence boundaries (SB, PSB1, PSB2, and PSB3) are superimposed. (For interpretation of the references to colour in this figure legend, the reader is referred to the Web version of this article.)

porosities and thus provide a better framework in conveying seismic signals compared to a more flexible micritic matrix (Jafarian et al., 2017a; Janson and Lucia, 2014) (Figs. 3, 9 and 10).

In the Kapp Starostin Formation, which is dominated by deeper and cold-water spiculitic chert horizons, the carbonate content increases towards the sequence tops as a result of third-order sea-level variations (Figs. 4 and 5). The parasequence boundaries PSB1, PSB2, and PSB3 are marked by an abrupt microfacies shift from carbonates to cherts (Figs. 4 and 5). Jafarian et al. (2017a) reported that an increment in carbonate content results in an increase of acoustic velocities. The carbonate-rich layers have higher bulk densities as well as velocities and consequently acoustic impedances compared to the surrounding chert units. The amplitude strength and polarity of the seismic traces are controlled by the relative difference in the acoustic properties at the transition between two sediment bodies (Nichols, 1999). Thus, independently of seismic frequency, a transition from carbonates to cherts creates the largest acoustic impedance contrasts and the pronounced seismic reflections (Figs. 3, 9 and 10).

These findings are in line with Zeller et al. (2015) who investigated Upper Jurassic to Lower Cretaceous shelf mixed carbonate – siliciclastic sediments in the Neuquén Basin (Argentina) that had a low-porosity domain (around 5%). The carbonate-rich sequence tops showed a higher acoustic impedance contrast with the surrounding siltstones and shales, which resulted in strong reflections within the synthetic seismograms.

In both investigated areas, the 200 Hz, 400 Hz and to a lesser extent 100 Hz profiles display an almost one to one relationship between the acoustic impedance models and the seismic events; SB, PSB1, PSB2, and PSB3 are at their true horizontal and vertical positions (Figs. 9 and 10). PSB1 that separates the outer ramp cherts of the Kapp Starostin Formation and the inner ramp carbonates of the Vøringen Member is the most robust feature that can be observed in all profiles (Figs. 9 and 10). Toward lower frequencies, 35–50 Hz, sequence/parasequence boundaries are obliterated (SB and PSB2) or show a mismatch with the outcrop equivalents (PSB3). The 25 Hz profiles do not provide insightful information on microfacies distribution and associated internal structures (Figs. 9 and 10).

As expected, the resolution problems and interference patterns decreases by an increment of the frequency (Figs. 9 and 10). The limited resolution of conventional industrial seismic wavelets precludes a one to one correspondence between the outcrop observations and seismic images. This is because of the wavelength of the seismic waves, which

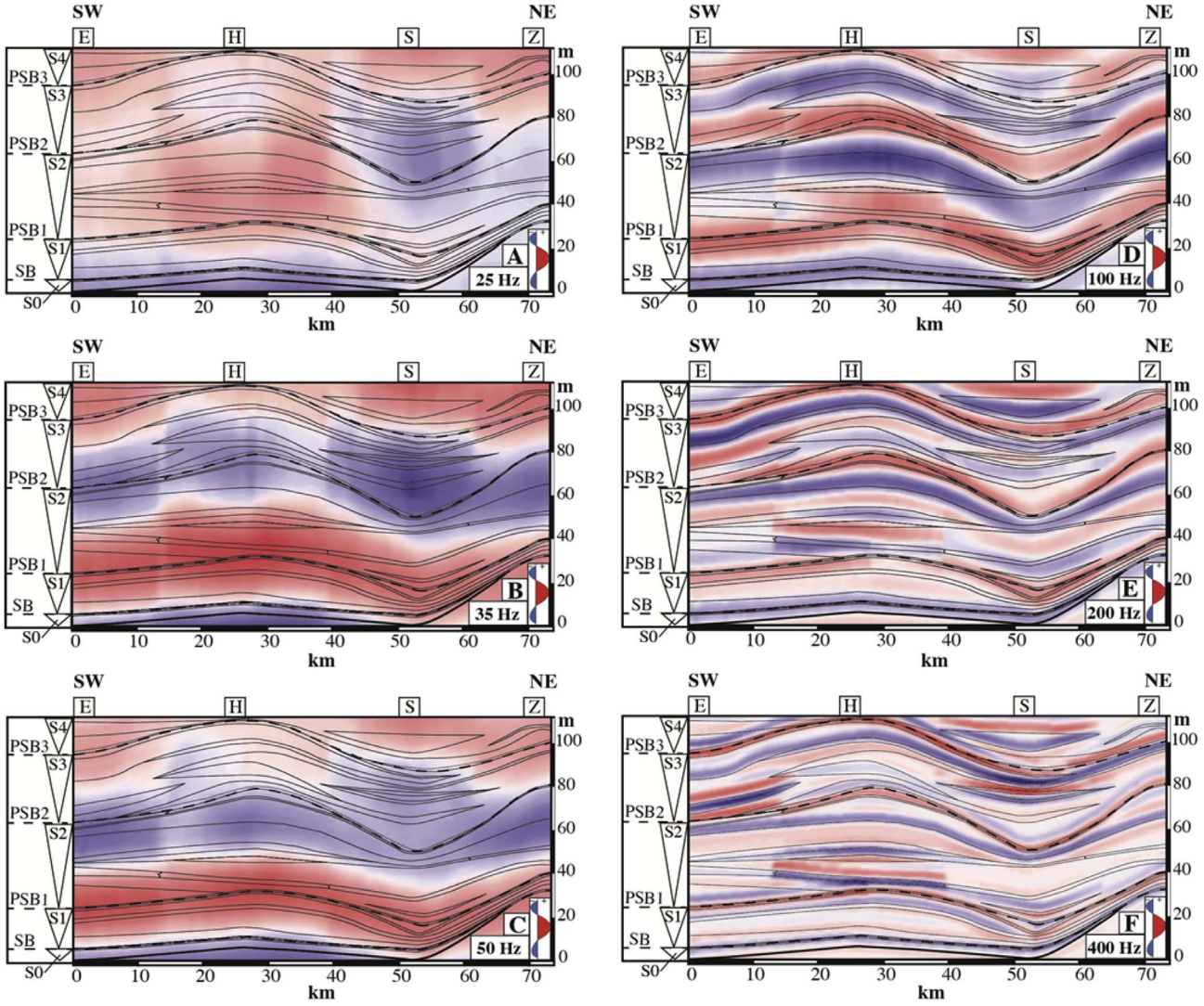

Fig. 10. Synthetic seismic profile at multiple frequencies (A: 25 Hz, B: 35 Hz, C: 50 Hz, D: 100 Hz, E: 200 Hz, F: 400 Hz) of NE Svalbard. Acoustic impedance values were used to calculate the reflection coefficients between the individual unit interfaces. Ricker wavelet (Ricker, 1953) was used for convolution to generate a synthetic seismic profile. The red colours are positive signals (hard-kick) and blue colours are negative signals (soft-kick). Sections location, microfacies transitions, defined third-order sequences (S0, S1, S2, S3, and S4) and sequence/parasequence boundaries (SB, PSB1, PSB2, and PSB3) are superimposed. (For interpretation of the references to colour in this figure legend, the reader is referred to the Web version of this article.)

Table 2
Summary of the carbonate producing factories information, averages of petrophysical properties and textural characteristics.

Carbonate producing factories	Dominant MFT	Dominant biota	Dominant diagenetic features	Texture	Average carbonate (%)	Average porosity (%)	Average Vp (40 MPa) (km/s)	Average Acoustic impedance (Nsm^{-3})
T-factory carbonates	MFTs- 6, 8	Algal mats, few sponge spicules, foraminifers, ostracods	Micritization	Mud-dominated	83.0	2.7	5.2	14.0
C-factory carbonates	MFTs- 5, 7 and 9	Brachiopods, bryozoans, echinoderms, sponge spicules	Chertification, Cementation	Grain-dominated	77.1	1.9	5.5	14.6

are too large to detect sediment heterogeneities on a meter-scale. In the low-frequency spectrum, higher-amplitude reflections might be caused by the occurrence of interference waves.

5.2. Relation to petrophysical properties

5.2.1. Porosity

It is known that porosity has a significant influence on acoustic velocities and impedance variations (Anselmetti and Eberli, 1993; Braaksma et al., 2003; Hossain and Zhou, 2015). Generally, with decreasing porosity and increasing density, velocity, and acoustic impedance increase.

In Miocene carbonates of the Cerro de la Molata platform (SE Spain; Kleipool et al., 2017) and Barremian-Aptian carbonates from the Provence (SE France; Fournier et al., 2014) with a high-porosity domain (0% to max 50%), porosity and pore types exert a significant, first-order

control on elastic properties.

The average porosity of the predefined microfacies is < 4%, except for the sandstone microfacies with an average of 11.8%. The acoustic impedance models of this study follow the density and porosity trends (Figs. 7 and 8). On Central Spitsbergen, Jafarian et al. (2017a) demonstrated that a decrease in velocity was accompanied by an increase in porosity. However, this negative trend is more evident for the relative high-porous samples (porosity > 5%; MFT-1: TR-1.41.1; MFT-3: KF-2.12.1; MFT-7: KF-1.6.1; and MFT-8: ID-1.4.1). This results in a high impedance contrast to surrounding non-porous layers and consequently high-amplitude reflections in the synthetic seismic seismograms (Fig. 3). For example, in section KF, PSB2 and PSB3 demonstrate the transition from porous massive cherts to bedded cherts by a strong negative reflection.

The wide scatter of values in velocity–porosity transforms can be caused by the type of pores (e.g., Xu and Payne, 2009; Zhao et al., 2013). Stiff pores, i.e., vuggy and moldic, can increment the pore space considerably without increasing the general elastic compressibility of the sediments. In contrast, a small fraction of crack-like pores results in softening the rock and reducing velocity (Xu and Payne, 2009; Zhao et al., 2013).

In the studied samples, the majority of the porosity is not visible in thin sections suggesting that it primarily occurs as micropores and microcracks. This finding is in agreement with the model of Xu and Payne (2009), which shows that crack-like pores dominate the pore space in this dataset diminishing acoustic velocity (Jafarian et al., 2017a). Hence, even in these relatively low-porous sediments, porosity still plays an important role controlling the acoustic properties, but the influence is less compared to datasets with wider porosity domains.

5.2.2. Mineralogy

The impact of mineralogy on the acoustic properties is well visible in sediments with limited porosity and pore types such as the studied dataset (Jafarian et al., 2017a; Kleipool et al., 2015). In this low-porous, biosiliceous – carbonate deposits, the seismic reflectors created with high-frequency wavelets (200–400 Hz) follow the spatial microfacies distribution within the defined parasequences (Figs. 9 and 10).

Since NE Svalbard is located in shallower depth, lower-order sea-level fluctuations associated with overall stormier, high-energy conditions locally disturb chert-dominated third-order sequences by the deposition of single limestone or sandstone beds (Blomeier et al., 2013; Jafarian et al., 2017b) (Fig. 5). Therefore, in this area, the contrast in mineralogy is significant within the individual parasequences, which are expressed as seismic reflectors in the 200 and 400 Hz profiles (Fig. 10). However, the seaward pinch-out of shallow-water deposits (limestone or sandstone) results in a momentary transition from bedded into massive cherts in Central Spitsbergen (Fig. 4). These subtle microfacies changes are marked by minor physical contrasts (Fig. 9). The low-resolution profiles (25–100 Hz) do not have the ability to resolve these microfacies alternating on a meter or sub-meter scale that occur within the lower-order sequences.

We can infer that the appearance of the seismic reflectors is primarily influenced by the high mineralogical contrasts of the defined facies, which variations are predominantly linked to relative sea-level fluctuations and, to a lesser extent, the sedimentary system. Due to variations in the spatial microfacies distribution, the proximal part displays higher internal amplitude contrasts with respect to the distal part (Figs. 3, 9 and 10). These observations are consistent with the results of Kleipool et al. (2015) who argued that high-amplitude contrasts in a low-porous mixed siliciclastic – carbonate ramp system (Upper Jurassic, Spain) are caused by the abrupt shifts in the type of the sediments. For the mixed carbonate – siliciclastic system of the Sobrarbe delta system (Pyrenees, N-Spain) with a domain porosity between 0 and 5%, De Jong (2015) also documented that the seismic traces follow the spatial microfacies distribution. Nevertheless, sediments of a single microfacies type with an almost given mineralogical composition (chert units in particular) show differences in acoustic impedance (Table 1). In the example shown in Fig. 3, PSB2 at section ID and KF representing the transition from massive to bedded cherts, however, shows different seismic signatures. This signifies internally non-homogeneous sediments, which most likely can be explained by the impact of visible and non-visible (microcrack) porosity or diagenetic alterations such as chertification and cementation that may enhance the seismic signal.

5.3. Seismic timeline and facies

Deposition and transportation of sediments within the C-factory are controlled by waves and currents resulting in a ramp-type morphology with continuous layer distribution. In the studied ramp system with overall limited lateral microfacies variations, significant changes in sediment composition and texture are coherent with the sequence/parasequence boundaries (e.g., carbonates-chert interfaces) (Figs. 4 and 5). These major transitions are mostly set to coincide with stratigraphic time surfaces. Consequently, the brightest seismic reflectors are coherent with both (Figs. 9 and 10). This is in line with the main premise in sequence stratigraphy that major stratal surfaces effectively signify geologic time surfaces. The latter is marked by sharp lithological contrast resulting from lateral shifts of the facies tracts (Van Wagoner et al., 1990). For the Bahamian T-Factory carbonate system, Eberli et al. (2001, 2002) showed that seismic reflections had chronostratigraphic significance. Sea-level fluctuations resulted in changes in sediment composition, sedimentation rate and diagenesis, which led to variations in sonic velocities, impedance contrasts and associated hard-kick and soft-kick seismic reflections (Eberli et al., 2001, 2002). Kleipool et al. (2017) proposed a conceptual model of the microfacies control on seismic reflectors within the C-factory. They noted that when cool-water carbonate factories are active, rapid microfacies shifts as a result of sea-level fluctuation are coherent with timelines and consequently with the main impedance boundaries. In contrast, shelf carbonate systems are marked by a complex geometry with high lithological and physical differences within a single microfacies tract, whereas lateral microfacies shifts tend to be gradational over large distances. Thus, seismic signatures follow microfacies boundaries instead of geological time surfaces.

In the Permian shelf-margin mixed sediments of the upper San Andres Formation (Last Chance Canyon, New Mexico) Stafleu and Sonnenfeld (1994) proposed two impedance models: (i) one with contrast at time-significant surfaces and, others (ii) with contrast at facies transitions. Comparison between these models and seismic line (placed around 50 km northwest of Last Chance Canyon) suggests that facies shifts, which are oblique to stratal surfaces, may be a prominent origin for seismic reflectors rather than time-significant surfaces. However, the resolution of stratal surfaces and facies shifts is intensely controlled by carbonate-sandstone alternations.

All in all, we can deduce that the type of carbonate factory, which is decisive for the platform morphology and consequently depositional character, controls the seismic reflection pattern.

5.4. Synthetic seismic profiles as analogue

The applicability of synthetic seismograms of outcrops and petrophysical data can be tested, if compared to time equivalent subsurface analogs (Bracco Gartner, 2000; Eberli et al., 2004).

The Upper Palaeozoic carbonate to biosiliceous successions of Svalbard occur along the entire Arctic shelf region and are known hydrocarbon plays on the Finnmark Platform, Loppa High and Sverdrup Basin (Ehrenberg et al., 2001; Golonka, 2002; Lerch et al., 2016). These deposits are characterized by a wide variability in petrophysical properties that hence introduce an additional uncertainty into seismic analyses.

The Templet Member analyzed in this study is the microfacies

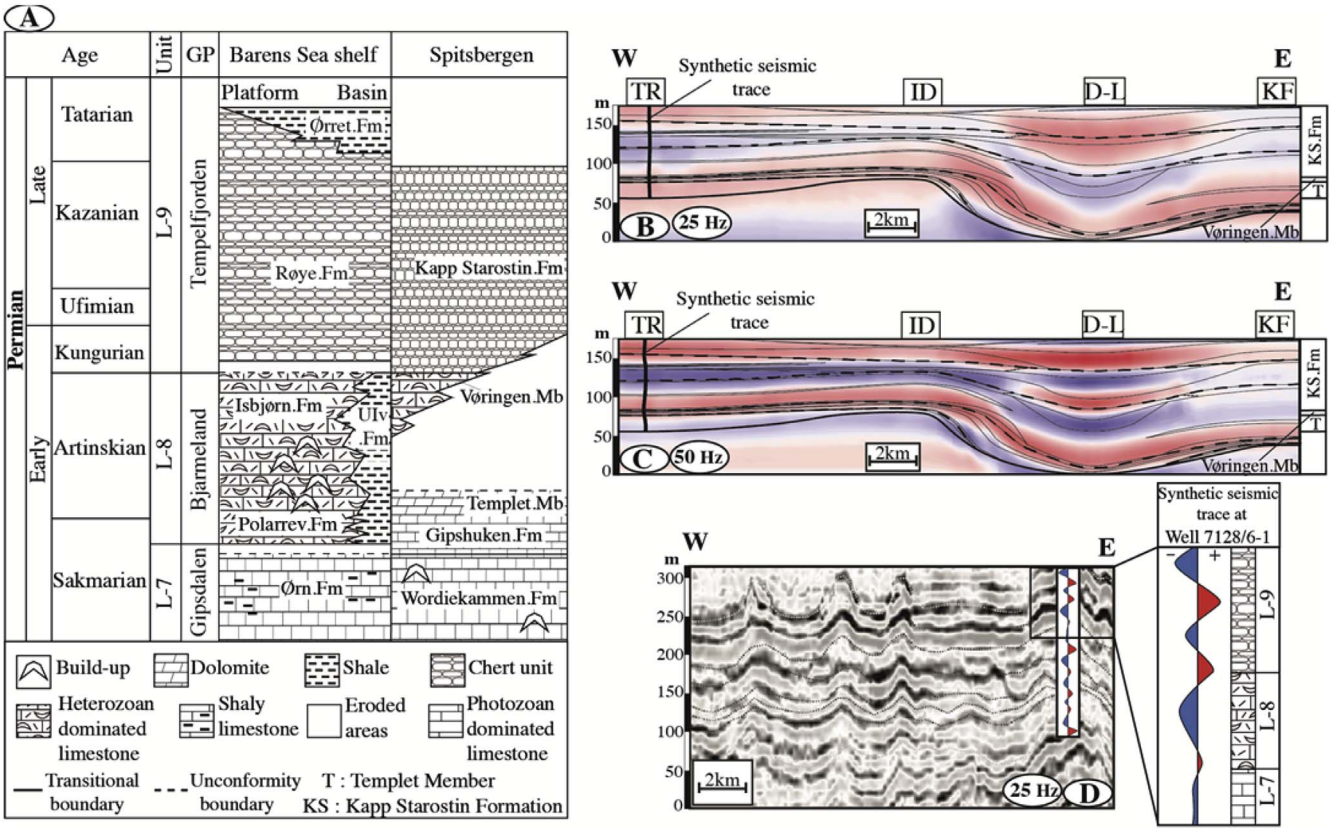

Fig. 11. A: The Upper Paleozoic lithostratigraphy of the Barents Sea Shelf and Spitsbergen (Colpaert et al., 2007; Ahlborn et al., 2014). B: the 1D synthetic seismic trace of the section TR (25 Hz) is superimposed on the 2D synthetic seismic profile (25 Hz) of Central Spitsbergen. C: the 1D synthetic seismic trace of section TR (50 Hz) is superimposed on the 2D synthetic seismic profile (50 Hz) of Central Spitsbergen. D: Synthetic seismic log (well 7128/6-1) and real seismic profile (25 Hz) of Finnmark platform (Colpaert et al., 2007).

equivalent of the tropical carbonates (foraminifera, algae) of unit L-7, but also time equivalent with the lower part of the overlying unit L-8 at the Finnmark Platform (Norwegian Barents Sea) (Fig. 11A). The top of unit L-8 consisting of heterozoan carbonates (e.g., crinoids, bryozoans, brachiopods) correlates with the Vøringen Member researched in this study, and lithological unit L-9 (Templefjorden group) is time and microfacies equivalent to the Kapp Starostin Formation (Jafarian et al., 2017b).

In the Finnmark Platform, Colpaert et al. (2007) studied the seismic sequence stratigraphy of the Upper Palaeozoic deposits by using 3D seismic data, and detailed lithostratigraphic studies resulting from well logs and cores. Based on well log data, synthetic seismic wavelets at 25 Hz frequency were constructed for correlation with the defined seismic sequences.

The thickness of the measured sections on Spitsbergen with at most 139 m falls below seismic resolution at real-frequency spectrum of 25 and 35 Hz. Therefore, the high-frequency wavelets (50–400 Hz) has been used for comparison with the real and synthetic seismic models of the Finnmark Platform of Colpaert et al. (2007) (Figs. 9 and 11). One needs to be aware that the continuous data of well logs, with approximately 50 cm vertical resolution, are more accurate for generating a seismic model, even at low-frequency wavelets, than data based on a limited number of samples. However, outcrop data do show lateral and vertical heterogeneity of the sediments due to the fine scale, data continuity and their 3D accessibility. Additionally, petrophysical data can be directly linked to sediment samples.

In the Finnmark Platform, the carbonate factory switching from tropical (unit L-7) to cool-water (unit L-8) is recognized by a low-amplitude positive signal in the real and synthetic seismic data (Colpaert et al., 2007) (Fig. 11D). On Spitsbergen, this boundary is obliterated at 25 Hz and showed a negative signal toward higher-frequency profiles (50–400 Hz) (Figs. 9 and 11B, C). A low-impedance interval at the basal transgressive sediments of unit L-8 could be related to the reworked lowstand deposits or higher shale content. These deposits are also present at the base of the Vøringen strata but thin out below seismic detectability.

The overlying cool-water grainstones (brachiopods, bryozoans, and echinoderms) of unit L-8 display high acoustic impedance values similar to the seismic expression of heterozoan carbonates in the Vøringen Member. The real seismic of unit L-8 shows mounded bryozoan build-up structures on the deeper-water slopes (Colpaert et al., 2007). These features were not observed on Spitsbergen since the study area was located in the shallower depositional setting during this period (Fig. 11B and C).

In the Finnmark Platform, the sharp interface between low-impedance cherts of unit L-9 (Average Vp: 5 km/s) and high-impedance carbonates of unit L-8 (Average Vp: 6 km/s) is marked by a distinct positive reflection in the synthetic and real seismic data (Fig. 11D). The seismic expression at this major microfacies shift is matched with the synthetic seismic signature at PSB1 of the present study (Figs. 9 and 11B, C). Based on subsurface seismic data of unit L-9, spiculites mounds occur along restricted zones that show internal variations in seismic reflections. The seismic behavior of the Kapp Starostin Formation also shows similar heterogeneities which originate from changes in lithology, porosity or the impact of a secondary process such as chertification (Figs. 9 and 11) (Colpaert et al., 2007). In the Finnmark Platform, isolated mounds as well as continuous buildup complexes of different sizes could cause the wavy character of seismic reflectors.

In summary, it can be deduced that there are no big impedance contrasts between the micrite-supported tropical carbonates of unit L-7 (the Gipsdalen Group, Average Vp: 6 km/s) and the grain-supported cool-water carbonates of unit L-8 (the Bjarmeland Group, Average Vp:

6 km/s) (Fig. 11D) (Rafaelsen et al., 2008). The distinct seismic events in the synthetic and real seismic data of the Finnmark Platform are caused by major shifts in the type of sediments, which are coherent with the cycle boundaries (e.g., carbonate – non carbonate shifts). These observations are in line with the findings of the present study and are also in agreement with the results of the seismic model of Rudolph et al. (1989). The latter showed that in regions of complex depositional architectures with abrupt microfacies changes, sequence boundaries might represent a simplified, but still valid version of the actual subsurface stratigraphy.

6. Conclusions

The goal of this study was to document the seismic expression of the Permian low-porous, biosiliceous – carbonate sediments, which were studied at several outcrops on Svalbard. The key findings of the transposition of the observed outcrop microfacies variations into synthetic seismograms at multiple frequencies are:

- The sequence stratigraphy documented in the outcrop can be linked to the reflectors in the synthetic seismic profiles produced with high-frequency wavelets (100–400 Hz).
- Conventional, low-frequency wavelets (25–50 Hz) have a resolution limitation and do not show a clear relationship between the Svalbard outcrop observations and the synthetic seismic profiles. However, some of the key surfaces (sequence/parasequence boundaries) can be identified in the real seismic spectrum but show a mismatch between the seismic reflectors and their outcrop equivalents.
- Abrupt microfacies transitions related to changes in sea level, followed by the amount of porosity and diagenetic effects such as cementation and chertification cause high-amplitude reflections in the synthetic seismic profiles. In the deeper and cold-water spiculites-dominated parasequences, the carbonate-rich sequence tops have strong seismic reflections in the synthetic seismic seismograms. The amount of porosity has the adverse effect on the acoustic velocities whereas carbonate content, cementation and chertification enhance the acoustic velocities and impedances in the present dataset.
- Within the C-carbonate factory, which is marked by lateral homogenous layers, major reflections are coherent with main facies shifts, thus sequence/parasequence boundaries and depositional timelines. In contrary, a facies dependent seismic signature would be expected in T-carbonate factory due to the lateral heterogeneity of the sediment within a single facies tract.
- Rapid changes in lithology and diagenetic overprints cause interference patterns resulting in a poor correlation between the synthetic seismograms and outcrop observations.
- Comparison with real seismic and synthetic seismic traces of the Finnmark Platform, a subsurface analogue with similar lithology, shows similarities in the seismic reflection patterns. This comparison confirms that major changes in the mineral composition of the sediments as a result of sea-level fluctuations are the main trigger for shifts in amplitude strength and polarity of the seismic traces.

Acknowledgements

Financial support of the Vrije Universiteit Amsterdam (the Netherlands), University of Bremen (Germany) and the Norwegian Polar Institute (Tromsø, Norway) is greatly acknowledged. Bouke Lacet and Wynanda Koot (Vrije Universiteit Amsterdam) are thanked for preparing the thin-sections and cylindrical plugs. We thank MSc. Students Ralph Groen, Mahtab Mozafari and Jan Schneider of the Vrije Universiteit Amsterdam for their contributions. We thank the College of Petroleum Engineering and Geosciences of the King Fahd University of Petroleum and Minerals (Kingdom of Saudi Arabia) for their support during the final stages of the manuscript. The constructive suggestions and comments of an anonymous reviewer contributed to a significant improvement of this paper. Finally Ronald J. Steel is thanked for his support as associate editor. This is CPG-CarbSed contribution no. 5.

References

Adam, L., Batzle, M., Brevik, I., 2006. Gassmann's fluid substitution and shear modulus variability in carbonates at laboratory seismic and ultrasonic frequencies. Geophysics 71, 173–183.
Ahlborn, M., Stemmerik, L., Kalsto, T.K., 2014. 3D seismic analysis of karstified interbedded carbonates and evaporites, lower permian gipsdalen group, Loppa high, southwestern Barents sea. Mar. Petrol. Geol. 56, 16–33.
Alves, F., Almeida, J.A., Silva, A.P., 2014. Simulation of acoustic impedance images by stochastic inversion of post-stack seismic reflection amplitudes and well data. J. Petrol. Sci. Eng. 121, 52–65.
Anselmetti, F.S., Eberli, G.P., 1993. Controls on sonic velocity in carbonates. Pure Appl. Geophys. 141, 287–323.
Bacon, M., Simm, R., Redshaw, T., 2007. 3-D Seismic Interpretation. Cambridge University Press, pp. 238.
Baechle, G., Weger, R., Eberli, G., 2005. Changes of shear moduli in carbonate rocks: implications for Gassmann applicability. The Leading Edge 24, 507–510.
Beauchamp, B., 1994. Permian climatic cooling in the Canadian Arctic. In: In: Klein, G. (Ed.), Pangaea: Paleoclimate, Tectonics, and Sedimentation during Accretion, Zenith, and Breakup of a Supercontinent, vol. 288. Geological Society of America Special Papers, pp. 229–246.
Beauchamp, B., Baud, A., 2002. Growth and demise of Permian biogenic chert along northwest Pangea: evidence for end– Permian collapse of thermohaline circulation. Palaeogeogr. Palaeoclimatol. Palaeoecol. 184, 37–63.
Beauchamp, B., Grasby, S., 2012. Permian lysocline shoaling and ocean acidification along NW Pangaea led to carbonate eradication and chert expansion. Palaeogeogr. Palaeoclimatol. Palaeoecol. 350–352, 73–90.
Blomeier, D., Dustira, A.M., Forke, H., Scheibner, C., 2011. Environmental change in the Early Permian of NE Svalbard: from a warm–water carbonate platform (Gipshuken Formation) to a temperate, mixed siliciclastic – carbonate ramp (Kapp Starostin Formation). Facies 57, 493–523.
Blomeier, D., Dustira, A.M., Forke, H., Scheibner, C., 2013. Facies analysis and depositional environments of a storm-dominated, temperate to cold, mixed siliceous–carbonate ramp: the Permian Kapp Starostin Formation in NE Svalbard. Norw. J. Geol. 93, 75–93.
Bourbié, T., Coussy, O., Zinszner, B., 1987. Acoustics of Porous Media. Gulf Publishing, Co, Houston TX, pp. 334.
Bracco Gartner, G.L., 2000. High Resolution Impedance Models of Outcrops and Their Applications in Seismic Interpretations. PhD Thesis. VU University Amsterdam, The Netherlands, pp. 144.
Braaksma, H., Kenter, J.A.M., Proust, J.N., Dijkmans, V., Van Hoek, T., Mahieux, G., Drijkoningen, G.G., 2003. Controls on acoustic properties of Upper Jurassic siliciclastic rocks (Boulonnais, northern France). Geophysics 68, 58–69.
Colpaert, A., Pickard, N., Mienert, J., Henriksen, L.B., Rafaelsen, B., Andreassen, K., 2007. 3D seismic analysis of an Upper Palaeozoic carbonate succession of the Eastern Finnmark platform area, Norwegian Barents Sea. Sediment. Geol. 197, 79–98.
Dallmann, W.K., Gjelberg, J.G., Harland, W.B., Johannessen, E.P., Keilen, H.B., Lønøy, A., Nilsson, I., Worsley, D., 1999. The upper palaeozoic lithostratigraphy. In: Dallmann, W.K. (Ed.), Lithostratigraphic Lexicon of Svalbard. Norsk Polarinstitutt, Tromsø, pp. 25–126.
De Jong, K., 2015. Synthetic Seismic Profile of Lateral Variations in the Sobrarbe Delta (Pyrenees, Northern Spain). Unpublished MSc Thesis. VU University Amsterdam, The Netherlands, pp. 56.
Eberli, G.P., Anselmetti, F.S., Betzler, C., Van Konijnenburg, J.H., Bernoulli, D., 2004. Carbonate platform to basin transitions on seismic data and in outcrops: great Bahama Bank and the Maiella platform margin, Italy. In: Eberli, G.P., Massaferro, J.L., Sarg, J.F. (Eds.), Seismic Imaging of Carbonate Reservoirs and Systems. vol. 81. AAPG Memoir, pp. 207–250.
Eberli, G.P., Anselmetti, F.S., Kenter, J.A.M., McNeill, D.F., Melim, L.A., 2001. Calibration of seismic sequence stratigraphy with cores and logs. In: In: Ginsburg, R.N. (Ed.), Subsurface Geology of a Prograding Carbonate Platform Margin, Great Bahama Bank: Results of the Bahamas Drilling Project, vol. 70. SEPM Special Publication, Tulsa, Oklahoma, USA, pp. 241–265.
Eberli, G.P., Anselmetti, F.S., Kroon, D., Sato, T., Wright, J.D., 2002. The chronostratigraphic significance of seismic reflectors along the Bahamas Transect. Mar. Geol. 185, 1–17.
Ehrenberg, S., Pickard, N., Henriksen, L., Svånå, T.A., Gutteridge, P., Macdonald, D., 2001. A depositional and sequence stratigraphic model for cold-water, spiculitic strata based on the Kapp Starostin Formation (Permian) of Spitsbergen and equivalent deposits from the Barents Sea. AAPG Bull. 85, 2061–2088.
Falivene, O., Arbues, P., Ledo, J., Benjumea, B., Munoz, J.A., Fernandez, O., Martinez, S., 2010. Synthetic seismic models from outcrop-derived reservoir-scale three-dimensional facies models: the Eocene Ainsa turbidite system (Southern Pyrenees). AAPG Bull. 94, 317–343.
Fournier, F., Borgomano, J., 2007. Geological significance of seismic reflections and imaging of the reservoir architecture in the Malampaya gas field (Philippines). AAPG Bull. 91, 235–258.
Fournier, F., Léonide, P., Kleipool, L., Toullec, R., Reijmer, J.J.G., Borgomano, J., Klootwijk, T., Van Der Molen, J., 2014. Pore space evolution and elastic properties of platform carbonates (Urgonian limestone, Barremian-Aptian, SE France). Sediment.

Geol. 308, 1–17.
Gassmann, F., 1951. Elastic waves through a packing of spheres. Geophysics 16, 673–685.
Golonka, J., 2002. Plate-tectonic maps of the phanerozoic. In: In: Kiessling, W., Flügel, E., Golonka, J. (Eds.), Phanerozoic Reef Patterns, vol. 72. SEPM Special Publications, Tulsa, Oklahoma, USA, pp. 21–70.
Groen, R.D., 2010. From a Restricted Carbonate Platform to a Temperate, Storm-dominated Ramp: the Onset of the Permian Chert Event in Central Spitsbergen. Unpublished MSc Thesis. VU University Amsterdam, The Netherlands, pp. 105.
Hodgetts, D., Howell, J.A., 2000. Synthetic seismic modelling of a large-scale geological cross-section from the Book Cliffs, Utah, USA. Petrol. Geosci. 6, 221–229.
Hossain, Z., Zhou, Y., 2015. Petrophysics and rock physics modelling of diagenetically altered sandstone. Interpretation 3, 107–120.
Jacquin, T., Arnaud-Vanneau, A., Arnaud, H., Ravenne, C., Vail, P., 1991. Systems tracts and depositional sequences in a carbonate setting: a study of continuous outcrops from platform to basin at the scale of seismic lines. Mar. Petrol. Geol. 8, 122–139.
Jafarian, E., Kleipool, L.M., Scheibner, C., Blomeier, D., Reijmer, J.J.G., 2017a. Variations in petrophysical properties of Upper Palaeozoic mixed carbonate and non–carbonate deposits, Spitsbergen, Svalbard Archipelago. J. Petrol. Geol. 40, 59–83.
Jafarian, E., Groen, R.D., Nooitgedacht, C.W., Scheibner, C., Blomeier, D.P.G., Reijmer, J.J.G., 2017b. Facies arrangement and cyclostratigraphic architecture of the Templet Member and the Kapp Starostin Formation (Permian) on Spitsbergen, Svalbard. Norw. J. Geol. 97 (4), 213–231.
Janson, X., Eberli, G.P., Bonnaffe, F., Gaumet, F., De Casanove, V., 2007. Seismic expressions of a Miocene prograding carbonate margin, Mut Basin, Turkey. AAPG Bull. 91, 685–713.
Janson, X., Lucia, F.J., 2014. Relationship between Acoustic and Petrophysical Properties of Permian Dolograinstones. pp. 40 Search and Discovery Article #41263.
Kenter, J., Bracco Gartner, G., Schlager, W., 2001. Seismic models of a mixed carbonate – siliciclastic shelf margin: permian upper san Andres Formation, Last chance Canyon, New Mexico. Geophysics 66, 1744–1748.
Kleipool, L.M., Reijmer, J.J.G., Bádenas, B., Aurell, M., 2015. Variations in petrophysical properties along a mixed siliciclastic carbonate ramp (Upper Jurassic, Ricla, NE Spain). Mar. Petrol. Geol. 68, 158–177.
Kleipool, L.M., De Jong, K., De Vaal, E.L., Reijmer, J.J.G., 2017. Seismic characterization of switching platform geometries and dominant carbonate producers (Miocene, Las Negras, Spain). Sedimentology 64, 1676–1707.
Lerch, B., Karlsen, D.A., Matapour, Z., Seland, R., Backer-Owe, K., 2016. Organic geochemistry of Barents Sea petroleum: thermal maturity and alteration and mixing processes in oils and condensates. J. Petrol. Geol. 39, 125–148.
May, B.T., Hron, F., 1978. Synthetic seismic sections of typical petroleum traps. Geophysics 43, 1119–1147.
Montgomery, S.L., 1998. Thirtyone formation, Permian Basin, Texas: structural and lithologic heterogeneity in a lower devonian chert reservoir. AAPG Bull. 82, 1–24.
Nakrem, H.A., Nilsson, I., Mangerud, G., 1992. Permian biostratigraphy of Svalbard (Arctic Norway) — a review. Int. Geol. Rev. 34, 933–959.
Nichols, G., 1999. Sedimentology and Stratigraphy, second ed. Wiley-Blackwell, Oxford, United Kingdom, pp. 419.
Rafaelsen, B., Elvebakk, G., Andreassen, K., Stemmerik, L., Colpaert, A., Samuelsberg, T.J., 2008. From detached to attached carbonate build-up complexes—3D seismic data from the Upper Palaeozoic, Finnmark Platform, southwestern Barents Sea. Sediment. Geol. 206, 17–32.
Ravenne, C., Vially, R., 1988. Observation of outcrops at a seismic scale in view of seismic stratigraphic interpretation. In: Guidebook of Fieldtrip 2, AAPG Mediterranean Basins Conference, Nice, pp. 52.
Reid, C.M., James, N.P., Beauchamp, B., Kyser, T.K., 2007. Faunal turnover and changing oceanography: late palaeozoic warm-to coolwater carbonates, Sverdrup Basin, Canadian Arctic archipelago. Palaeogeogr. Palaeoclimatol. Palaeoecol. 249, 128–159.
Ricker, N., 1953. The form and laws of propagation of seismic wavelets. Geophysics 18, 10–40.
Rudolph, K.W., Schlager, W., Biddle, K.T., 1989. Seismic models of a carbonate foreslope-to-basin transition, Picco di Vallandro, Dolomite Alps, northern Italy. Geology 17, 453–456.
Schoenberger, M., 1974. Resolution comparison of minimum-phase and zero-phase signals. Geophysics 39, 826–833.
Schwab, A.M., Cronin, B.T., Ferreira, H., 2007. Seismic expression of channel outcrops: offset stacked versus amalgamated channel systems. Mar. Petrol. Geol. 24, 504–514.
Scotese, C.R., Langford, R.P., 1995. Pangaea and the paleogeography of the permian. In: In: Scholle, P.A., Peryt, T.M., Ulmer-Scholle, D.S. (Eds.), The Permian of Northern Pangaea, Paleogeography, Paleoclimates, Stratigraphy, vol. 1. Springer, Berlin Heidelberg New York, pp. 3–19.
Schlager, W., 2005. Carbonate sedimentology and sequence stratigraphy. SEPM Concepts in Sedimentology and Paleontology, vol. 8. pp. 200 Tulsa, Oklahoma, USA.
Stafleu, J., 1994. Seismic Models of Outcrops as an Aid in Seismic Interpretation. PhD Thesis. VU University, Amsterdam, The Netherlands, pp. 223.
Stafleu, J., Everts, A.J., Kenter, J.A., 1994. Seismic models of a prograding carbonate platform: Vercors, south-east France. Mar. Petrol. Geol. 11, 514–527.
Stafleu, J., Sonnenfeld, M.D., 1994. Seismic models of a shelf margin depositional sequence: upper san Andres Formation, Last chance Canyon, New Mexico. J. Sediment. Res. 64, 481–499.
Stemmerik, L., Worsley, D., 1989. Late palaeozoic sequence correlations, North Greenland, Svalbard and the Barents shelf. In: Collinson, J.D. (Ed.), Correlation in Hydrocarbon Exploration. Norwegian Petroleum Society, Graham & Trotman, London, pp. 99–111.
Van Wagoner, J.C., Mitchum, R.M., Campion, K.M., Rahmanian, V.D., 1990. Siliciclastic sequence stratigraphy in well logs, cores, and outcrops: Concepts for high-resolution correlation of time and facies. In: AAPG Methods in Exploration, vol. 7. AAPG, Tulsa, pp. 55.
Xu, S., Payne, A.M., 2009. Modeling elastic properties in carbonate rocks. Lead. Edge 28, 66–74.
Zeller, M., Eberli, G.P., Weger, R.J., Giunta, D.L., Massaferro, J.L., 2014. Seismic expressions of the Quintuco e Vaca Muerta system based on outcrop facies and geometry. In: IX Congreso de Exploración y Desarrollo de Hidrocarburos, Simposio de Recursos No Convenionales: Ampliando el Horizonte Energético, pp. 209–224.
Zeller, M., Reid, S.B., Eberli, G.P., Weger, R.J., Massaferro, J.L., 2015. Sequence architecture and heterogeneities of a field-Scale Vaca Muerta analog (Neuquén Basin, Argentina) - from outcrop to synthetic seismic. Mar. Petrol. Geol. 66, 829–847.
Zhao, L., Nasser, M., Han, D., 2013. Quantitative geophysical pore-type classification and its geological implication in carbonate reservoirs. Geophys. Prospect. 61, 827–841.